Weather & Climate

JOURNAL OF THE METEOROLOGICAL SOCIETY OF NEW ZEALAND (INC.)

VOLUME 38 • ISSUE 1 • 2018

WEATHER & CLIMATE

JOURNAL OF THE METEOROLOGICAL SOCIETY OF NEW ZEALAND (INC.)

VOLUME 38 ● ISSUE 1 ● 2018

ISSN 0111-5499

Weather and Climate is the official journal of the Meteorological Society of New Zealand (Inc.). Any opinions, statements or recommendations expressed in this journal are those of the respective author(s) and do not necessarily reflect the views of the Meteorological Society of New Zealand (Inc.).

Contributions to Weather and Climate are welcome on any meteorological or climatological subject, but preference will be given to contributions related to New Zealand and/or the Southwest Pacific.

Submissions can be made via Scholastica at: https://weather-and-climate.scholasticahq.com/ or by emailing the editor at nava.fedaeff@niwa.co.nz

EDITOR Nava Fedaeff

COVER IMAGE Eleanor Treadwell

Published: December 2018

Copland Track tramp. The clouds cleared whilst crossing the bridge to reveal the Copland river and the Rata.

THE METEOROLOGICAL SOCIETY OF NEW ZEALAND (INC.)

The Meteorological Society of New Zealand (Inc.) was inaugurated in October 1979. The objects of the Society are to encourage an interest in the atmosphere, the weather and the climate, particularly in the New Zealand and South Pacific regions. Membership is open to all those with an interest in the objects of the Society. Membership comprises both professionals and amateurs including meteorologists, climatologists, geographers, hydrologists, yachting and tramping enthusiasts, glider pilots, people involved in aviation and marine industries, agriculturalists, professional weather forecasters, ecologists, economists, farmers, engineers and weather observers.

Membership fees:

Ordinary members	$40.00
Student members	$20.00
Institutional members	$120.00
Overseas postage surcharge	$15.00

All members receive copies of Weather and Climate and the quarterly Newsletter (which includes details of significant weather events in the previous period).

Correspondence:
The Secretary
Meteorological Society of New Zealand
PO Box 6523, Marion Square, Wellington, 6141, New Zealand
Web site: http://metsoc.rsnz.govt.nz.

Officers of the Society for 2018

President	Sylvia Nichol
Immediate Past President	Daniel Kingston
Auckland VP	Petra Pearce
Hamilton VP	Tim Gunn
Wellington VP	James Renwick
Christchurch VP	Jiawei Zhang
Dunedin VP	Daniel Kingston
Secretary	Katrina Richards
Treasurer	Gregor Macara
Circulation Manager	Lisa Murray
Journal Editor	Nava Fedaeff
Newsletter Editor	Bob McDavitt
Website Liaison	Stefanie Kremser
General Committee	Mike Revell, Michael Martins, Ciaran Doolin, Luke Sutherland-Stacey, Charles Pearson

WEATHER & CLIMATE

JOURNAL OF THE METEOROLOGICAL SOCIETY OF NEW ZEALAND (INC.)

VOLUME 38 ● ISSUE 1 ● 2018

High resolution precipitation fields for the Clutha catchment

A. M. Jobst[1], D. G. Kingston[1] and N. J. Cullen[1]

[1] *Department of Geography, University of Otago, PO Box 56, Dunedin, New Zealand*

Correspondence: andijobst@gmail.com

Key words: precipitation, alpine catchment, interpolation, water balance, hydrological model, New Zealand

Abstract

NIWA's Virtual Climate Station Network (VCSN) is currently the only product that offers interpolated daily precipitation data for the whole of New Zealand. The VCSN has been used to successfully model hydrological processes in several catchments but it still contains significant biases for high elevation catchments. In this study, an attempt was made to create improved daily precipitation fields for New Zealand's largest catchment, the Clutha River. The grids have a higher spatial resolution than the VCSN (1 km^2 vs. ~5 km^2) and were created using a trivariate thin plate spline based on a modified version of the 30-year rainfall normal surface that was used as part of the VCSN approach. The original rainfall surface was adjusted because a water balance validation with the hydrological model WaSiM revealed substantial biases in several sub-catchments of the upper Clutha (from -13% to +72%). After the correction, the 20-year water balance error (1992-2012) did not exceed ±5% at any of the streamflow gauges used. Compared to the fields generated here, the annual precipitation of the VCSN is generally lower with the largest differences in the headwaters (> -2000 mm). Consequently, when compared to the VCSN the mean annual precipitation averaged across the Clutha catchment was found to be higher in this study (1415 mm vs. 1258 mm).

1. Introduction

The spatial distribution of precipitation across the South Island of New Zealand is characterised by large variability. While correct representation of daily precipitation is key for hydrological modelling studies (Tait et al., 2012), sparse station networks can hamper the generation of realistic spatial estimates. In addition to the common problem of insufficient data availability in alpine catchments (Suprit and Shankar, 2008; Schönbrodt-Stitt et al., 2013), wind-driven undercatch and evaporation can cause systematic measurement errors (Mekis and Hogg, 1999). Such errors can then negatively affect the performance of hydrological models (Oudin et al., 2006).

In the Southern Alps the highest annual totals tend to occur approximately 20 km upwind of the main divide (Wratt et al., 2000), which is a direct result of the interaction of a predominantly westerly airflow and the orography. Besides very high amounts of orographic precipitation to the west of the main divide, strong transmountain winds can cause large amounts of precipitation to fall on

Submitted: 12 September 2018
Accepted: 8 October 2018

the leeward side and this so-called spillover can extend up to 20 km eastwards from the main divide (Sinclair et al., 1997). With spillover being the dominant source of precipitation for the headwater catchments to the east of the main divide, the correlation between precipitation and elevation for the Southern Alps is rather weak by global standards (Wratt et al., 2000; Tait et al., 2006).

To provide input for hydrological models and other environmental applications Tait et al. (2006) estimated daily rainfall on a 0.05° grid (VCSN) for the whole of New Zealand using a trivariate thin-plate spline (TS). The TS was found to perform best if a rainfall normal surface was used as an independent covariable instead of elevation, which highlights the alternative role of the Southern Alps when compared to other alpine regions in terms of precipitation – elevation relationships (Lauscher, 1976; Marke, 2011). While the VCSN fields constitute a valuable data set for modelling studies in New Zealand, the use of independent regional council data highlighted that the daily fields still have significant errors in some regions of the Southern Alps with monthly mean absolute errors between 30 and 100 mm (Tait et al., 2012).

This study focuses on the Clutha catchment, which is New Zealand's largest catchment by area and mean flow. The Clutha's natural water resources are used extensively for hydropower generation and irrigation schemes. As part of a wider hydrological modelling study (Jobst et al., 2018) an attempt was made to improve on the VCSN and provide a more realistic precipitation input for a fully distributed hydrological model. A similar approach as described in Tait et al. (2006) was adopted to generate daily grids at the required spatial resolution of 1 km^2 between 1990 and 2012. The main differences between the VCSN approach and this study are the higher spatial resolution, a small number of additional precipitation records (i.e. regional council data) and a modified version of the 30-year (1951-1980) rainfall normal surface (as described in Tait et al. (2006)) that is used as part of the TS interpolation. Biases were assessed using a water balance approach in combination with the fully distributed hydrological model WaSiM (Schulla, 2012).

2. Methods

2.1 Data sources

A total of 76 sites with variable record lengths were included for the interpolation of daily precipitation (Figure 1). The majority of the sites are operated by NIWA (73) and three additional records were provided by the Otago Regional Council (ORC). Compared to the low number of sites recording temperature in the domain (Jobst et al., 2017), the precipitation network is more extensive and covers most parts of the Clutha catchment. However, most of these sites are located in intermontane valleys and the upper headwaters that originate downwind from the main divide (~0-12 km) can be considered ungauged, with the only exception being the relatively short record (~4 years) at Young River (P-O1). In Figure 2 the mean annual precipitation totals of all 76 records are plotted against the corresponding distances to the main divide. The highest totals were recorded at the two Milford Sound sites (P-N3 and P-N4), while the shorter P-O1 record has the highest annual precipitation (> 5000 mm) of any site inside the watershed. Further inland and towards the east coast, precipitation totals decrease rapidly and remain below 1000 mm at most sites.

2.2 Extension of the Young River precipitation record

The rainfall station at P-O1 (operated by ORC) is located approximately 4 km to the lee of the main divide. The record is especially important as it is the only station within close proximity of the main divide, a zone where the intensity of spillover is expected to be strongest. To maximize the usage of the site's relatively short record (1/9/2008 – 1/9/2013) linear regression was used to extend the record through the remaining time period

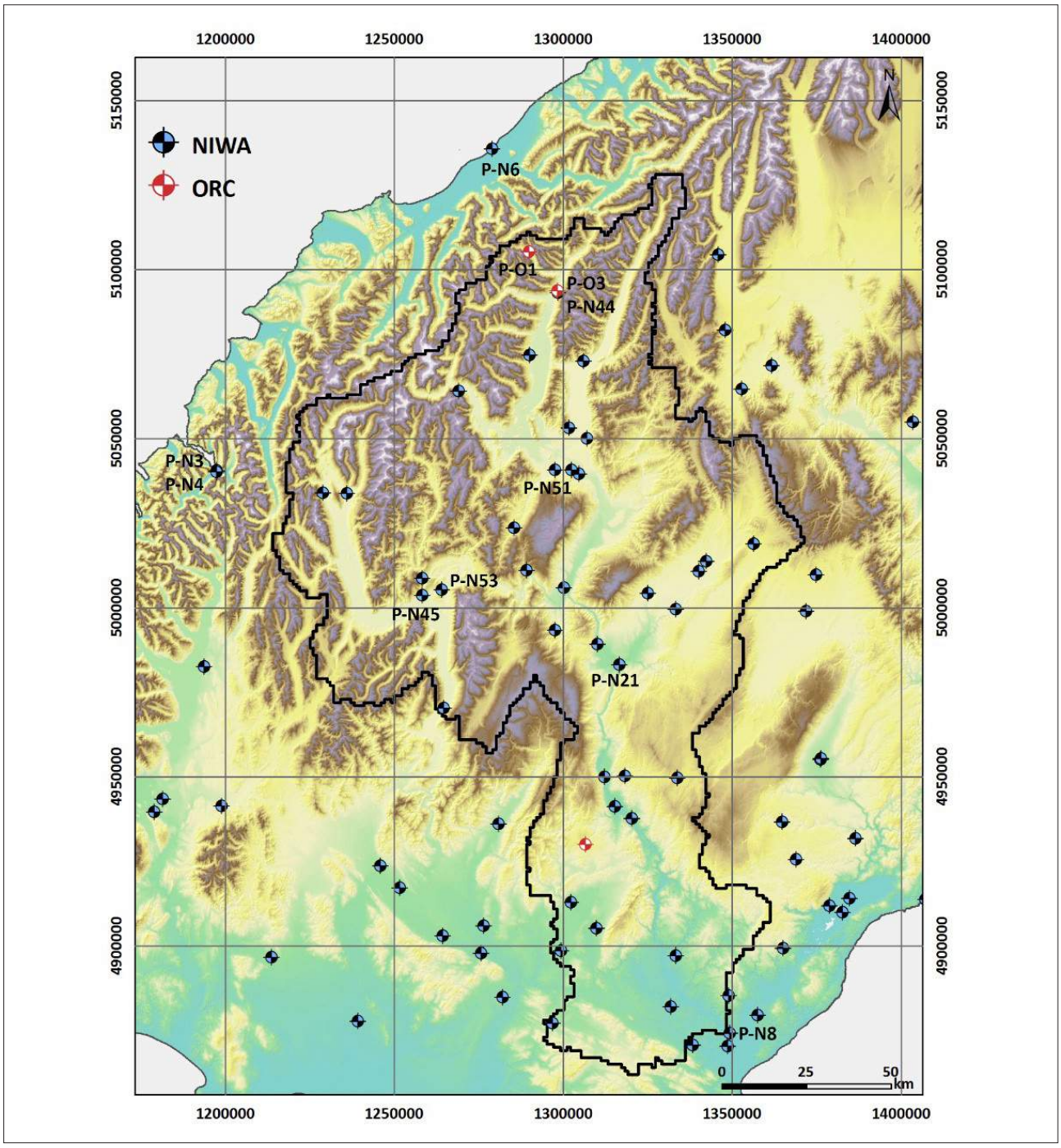

Figure 1: NIWA and ORC precipitation sites used for the daily interpolation. Mean annual precipitation of the labelled sites is shown in Figure 2 (note that site P-N44 is occluded by P-O3). The black line shows the Clutha catchment with the gauge in Balclutha as the outlet.

(1/4/1992 – 31/8/2008). The first regression (Equation 1) is based on the ORC site P-O3 at Makarora (15 km SE), which is the same rainfall station used by Cullen and Conway (2015) to reconstruct precipitation at Brewster Glacier. Importantly, P-O3 has the same tipping bucket instrument as the P-O1 site. Given that the record of P-O3 only dates back to 5/11/1997, the record of a manual daily rain gauge (P-N44), which is operated by

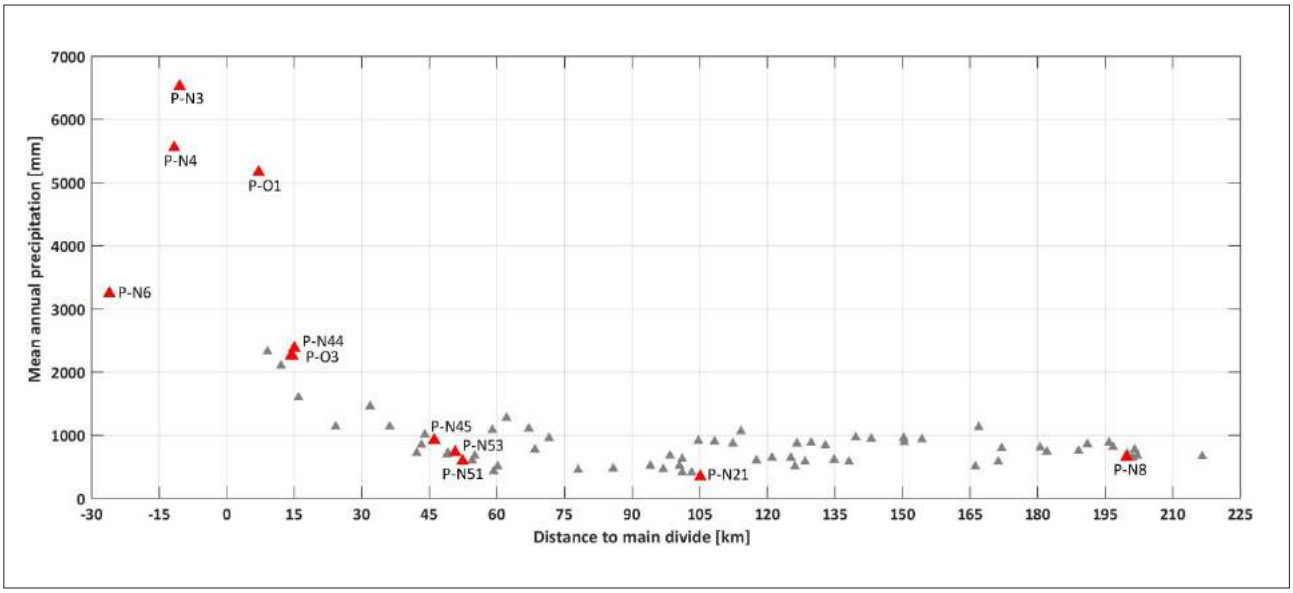

Figure 2: Mean annual precipitation (regular year) of all sites between 1992 and 2011 (shorter records are also plotted, e.g. P-O3 1998-2011) against distance to main divide. The location of the labelled sites (red triangles) is also shown in Figure 1.

NIWA and located approximately 500m from site P-O3, was used for the second regression (Equation 2), covering the remaining time period.

$$P\text{-}O1_{extended1} = 2.0308 * MAKARORA_{ORC} + 1.3282 \quad (1)$$

$$P\text{-}O1_{extended2} = 1.5643 * MAKARORA_{NIWA} + 4.0276 \quad (2)$$

Further, any scaled values were set to 0 mm if no precipitation was recorded for that time step. The calibration and validation periods were defined from 1/9/2008 to 31/8/2011 and from 1/9/2011 to 1/9/2013, respectively. The performance of the two best-fit regression models can be seen in Table 1 and Figure 3, where the first regression model (Equation 1) was found to have a better fit during both the calibration and validation period.

2.3 Undercatch correction step

Before the interpolation was carried out, a wind-dependent undercatch correction was performed. The empirical approach of Yang et al. (1998), which has been used by Kerr et al. (2011) in the Lake Pukaki catchment requires mean temperature and wind speed at the gauge height as input, and differentiates between solid, mixed and liquid precipitation. As most of the precipitation sites in the Clutha domain do not record wind speed or air temperature, daily fields of these two variables were instead used. A total of 22 stations were used for the interpolation of air temperature and 26 sites for wind speed (with only 13 stations located inside the catchment and only 7 stations covering the entire data period). The daily temperature grids were presented in Jobst et al. (2017) and are based on a TS and a monthly lapse rate

Table 1: Validation of the two regression models $P\text{-}O1_{extended1}$ and $P\text{-}O1_{extended2}$. Performance criteria (R2 and RMSE) were calculated for the calibration (CAL) and validation (VAL) period, respectively.

Scaled site	R^2 (CAL)	R^2(VAL)	RMSE(CAL)	RMSE(VAL)	Extension period
$P\text{-}O1_{extended1}$	0.90	0.85	10.10	12.05	05/11/1997-31/08/2008
$P\text{-}O1_{extended2}$	0.59	0.60	20.20	19.43	01/04/1992-04/11/1997

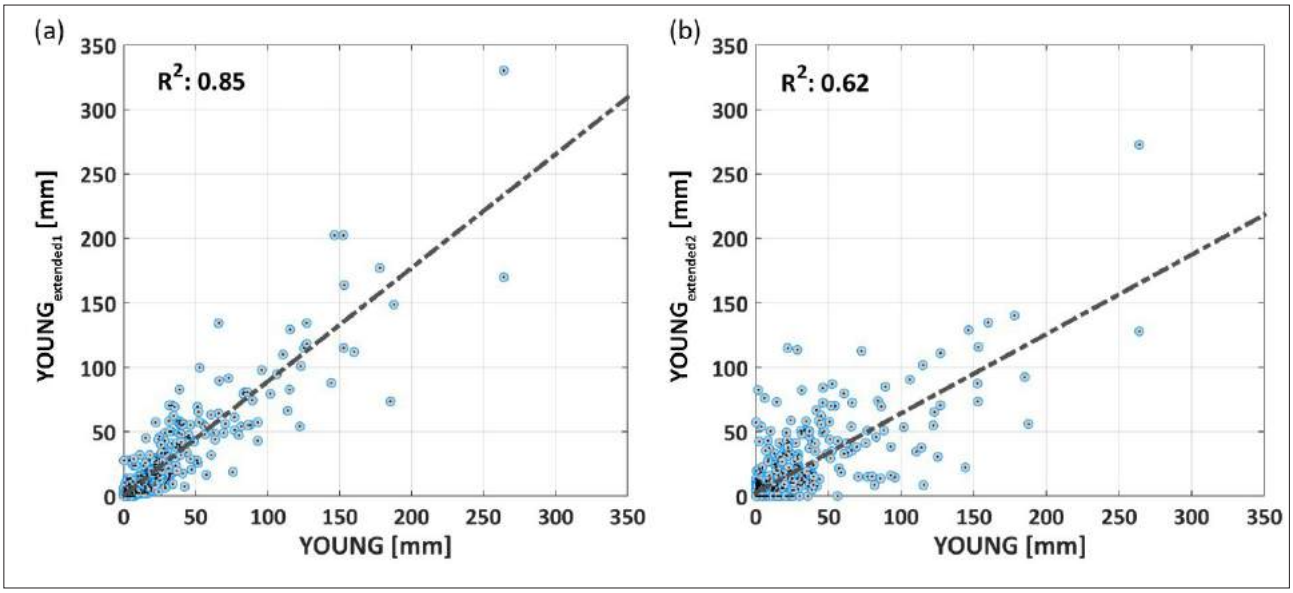

Figure 3: Scatterplots showing daily precipitation between YOUNG (= Site P-O1) and $YOUNG_{extended}$ during the validation period (1/9/2011 to 1/9/2013) for (a) the $P\text{-}O1_{extended1}$ and (b) the $P\text{-}O1_{extended2}$ regression model. The dashed line represents the line of best-fit.

model. The wind fields were generated using an elevation based TS run on a relatively sparse network of wind gauges.

2.4 Validation using water balance approach

After the undercatch correction, the 30-year rainfall normal surface was iteratively adjusted using a water balance approach and the assumption that natural stores of water are equal to zero over longer time periods. The fully distributed hydrological model WaSiM was used as a tool to approximate the true mean annual precipitation of the Clutha basin on a sub-catchment scale. The WaSiM model (described in Jobst et al. (2018)) models potential evapotranspiration via the Penman-Monteith approach, which is limited by soil water content and capillary pressure resulting in actual evapotranspiration (AET). Changes in the snow, unsaturated soil and groundwater stores are unlikely to have a significant effect on the water balance over the 20-year period. The same holds for the relatively small volume of glaciers located in the headwaters of the Clutha covering only ~0.7% (i.e. ~147 km^2) of the catchment (Chinn, 2001). This restricts the uncertainty introduced by WaSiM to the term of AET, which was computed at 518 mm. This number agrees well with the 540 mm estimate that Sirguey (2009) used for the upper Waitaki catchment and which is based on the averages of three Southern Alps studies (Anderton, 1974; Fitzharris and Garr, 1995; McKerchar and Pearson, 1997). Consequently, the error between observed and modelled streamflow was then assigned to over or under estimations of annual precipitation totals in the corresponding sub-catchments. The water balance validation was carried out over a 20-year period (1/4/1992-31/3/2012) for eight streamflow gauges, with the threshold for error (stopping criterion) defined as not being allowed to exceed ±5% at any of the sites.

A pragmatic approach was used to adjust the original rainfall normal surface ($SURF_{org}$) using a sub-catchment based correction factor grid. Biases in $SURF_{org}$ were assumed to be greater close to the main divide due to a lack of rain gauges and the steep gradient in spillover precipitation leeward from the main divide. From the main divide to the end of the spillover zone correction factors were thus reduced or increased linearly to one.

The spillover zone was defined between 0 and 24 km from the main divide based on the findings of Chater and Sturman (1998). Their study focused on the Waimakariri catchment, which is located at a relatively large distance (~200 km) to the northeast of the Clutha but has a comparable elevation range and is therefore assumed to have similar orographic uplift. Further linear factors were assigned to sub-catchments further inland. In order to create smooth transitions between neighbouring sub-catchments correction factors were assigned to the cells of the stream network, which were interpolated resulting in a continuous correction grid. The grid was then multiplied with $SURF_{org}$ to produce the adjusted rainfall surface ($SURF_{mod}$) and the TS was then rerun with $SURF_{mod}$ as the covariate.

3. Results

3.1 The water balance validation

The water balance validation of TS_{org} (TS using the $SURF_{org}$ shown in Figure 4) revealed substantial over- and underestimations of streamflow (and consequently precipitation) in several sub-catchments (Figure 5). The largest positive bias (72%) was calculated for the Shotover River at Peat's Hut (Shotover at Bowens Peak: 61%). As shown by Figure 4, $SURF_{org}$ reaches high totals exceeding 4000 mm in the upper ranges of the Shotover (indicated by white arrow). This local maximum shows substantially higher totals than other parts of the upper Clutha that are at a similar distance to the main divide. The spatial pattern of $SURF_{org}$ clearly follows the terrain of the upper Shotover, which has a plateau-like shape and on average reaches higher elevations than the neighbouring sub-catchments. During the expert guided process underlying the generation of $SURF_{org}$, a strong orographic effect must have been expected to enhance precipitation in the ungauged ridges of the upper Shotover (Tait et al., 2006). However, the large positive bias in Figure 5 appears to contradict this assumption.

For the Kawarau catchment opposing biases were found for the gauges at Frankton (9%) and The Hillocks (-5%). The positive bias at Frankton (Lake Wakatipu outlet) points to a substantial overestimation of precipitation in the remaining Wakatipu tributaries south of the Hillocks. The streamflow error was also found to be positive for Lake Wanaka (5%) and Lake Hawea (20%). Further inland, a relatively large positive bias (18%) was found for the intermontane Nevis valley, while the bias in the

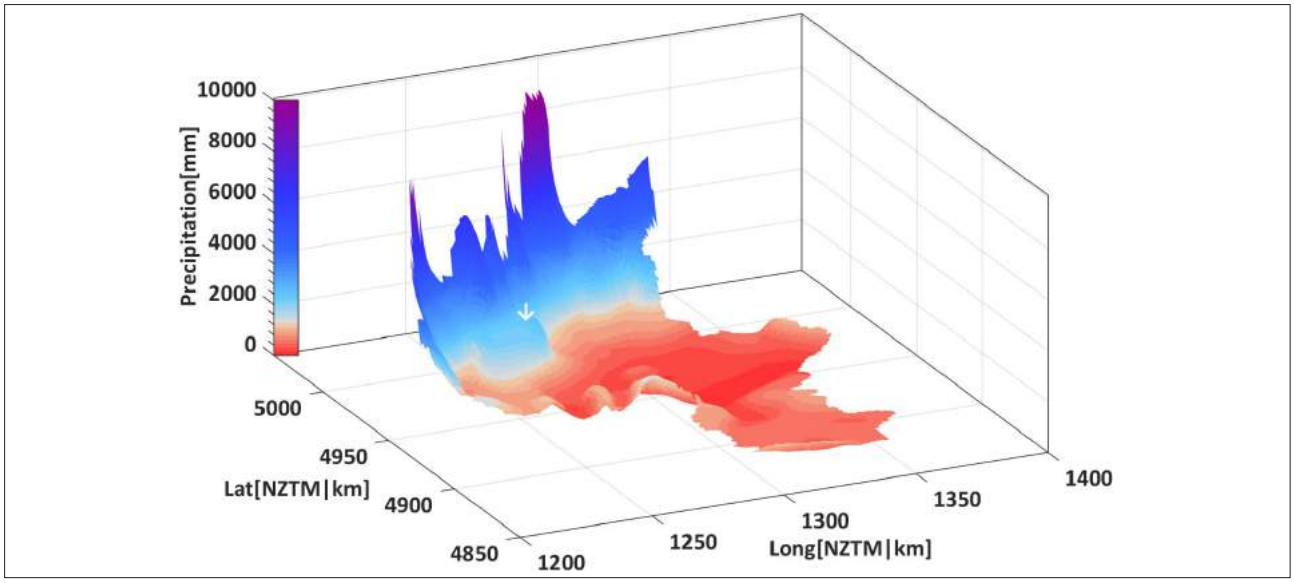

Figure 4: The original rainfall normal surface ($SURF_{org}$) clipped by the Clutha watershed (arrow points to the upper Shotover sub-catchment).

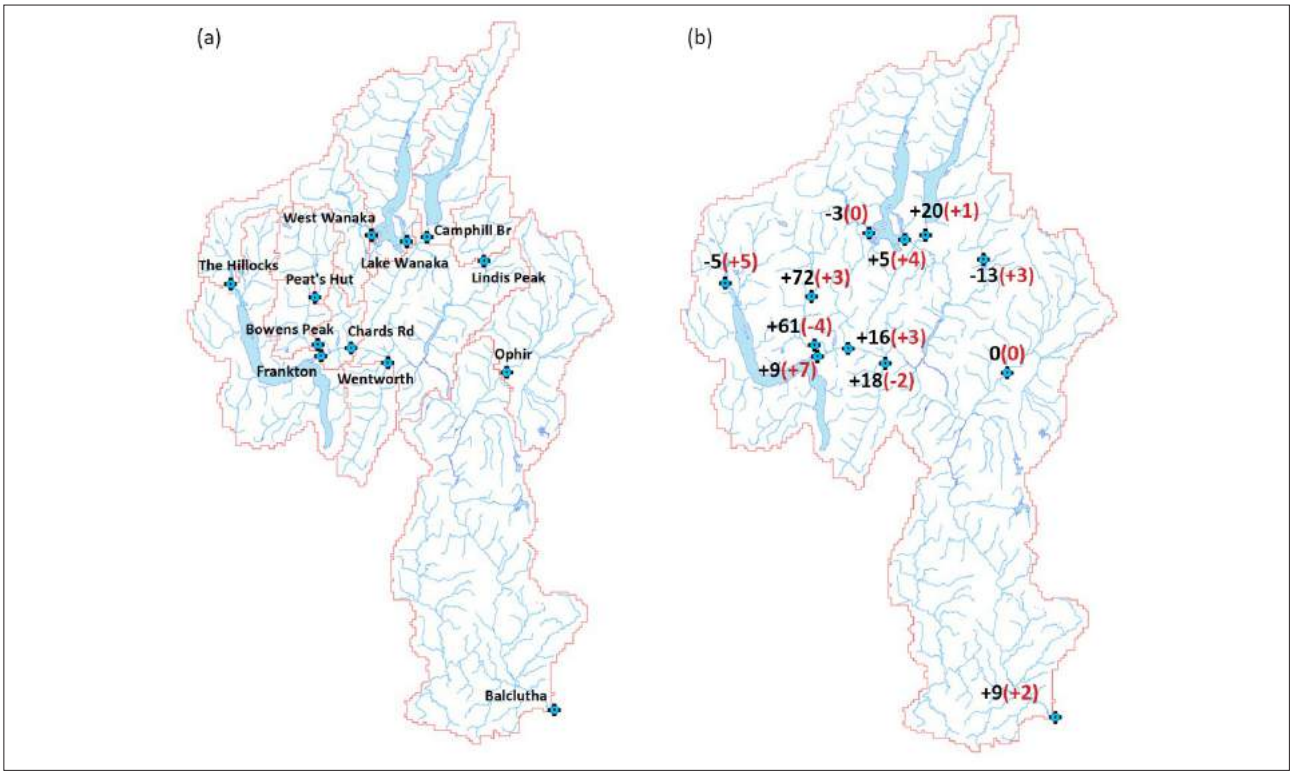

Figure 5: (a) The network of flow gauges and their corresponding sub-catchments (sub-catchments were derived using the topography based tool TANALYS (Schulla, 2012)). (b) The errors (%) between modelled and observed mean annual streamflow (1/4/1992 – 31/3/2012) for the TS_{org} forced run (black) and the TS_{mod} forced run (red).

upper Lindis (Lindis Peak) was negative (-13%). At the catchment's outlet (i.e. Balclutha) the combined upstream errors resulted in a substantial positive bias of 9%.

The final correction factor grid that was used to adapt $SURF_{org}$ (Figure 6a) has values ranging from 0.45 (Shotover) to 1.15 (The Hillocks). Correction factors tend steeply towards 1 when adjoining an area of the catchment that did not require correction. The factor grid was then multiplied with $SURF_{org}$ resulting in $SURF_{mod}$, with the difference between the two surfaces unfolded by Figure 6b.

As shown in Figure 5b (red font) the use of $SURF_{mod}$ as a covariate in the TS interpolation (TS_{mod}) led to a much more realistic simulation of streamflow. The most obvious difference between the two surfaces is the reduction of precipitation in the upper Shotover (Figure 6b), where the leeward extension of the high precipitation zone from the main divide has been substantially reduced, eliminating the previously large overestimation of observed streamflow. For all of the remaining sub-catchments with 20-year records the biases also remained within ±5%.

3.2 The annual catchment precipitation

Based on the daily fields created in this study, most of the Clutha catchment has annual precipitation of less than 1000 mm with the driest areas in the centre receiving less than 500 mm per year (Figure 7). At an approximate distance of 40 km from the main divide, annual totals exceed the catchment average (1415 mm; see dashed contour line) and increase rapidly until reaching 4000 mm between 2 and 10 km from the main divide. The highest precipitation totals ranging from 4000 mm to 10000 mm (exceeding 10000 mm in isolated cells) are

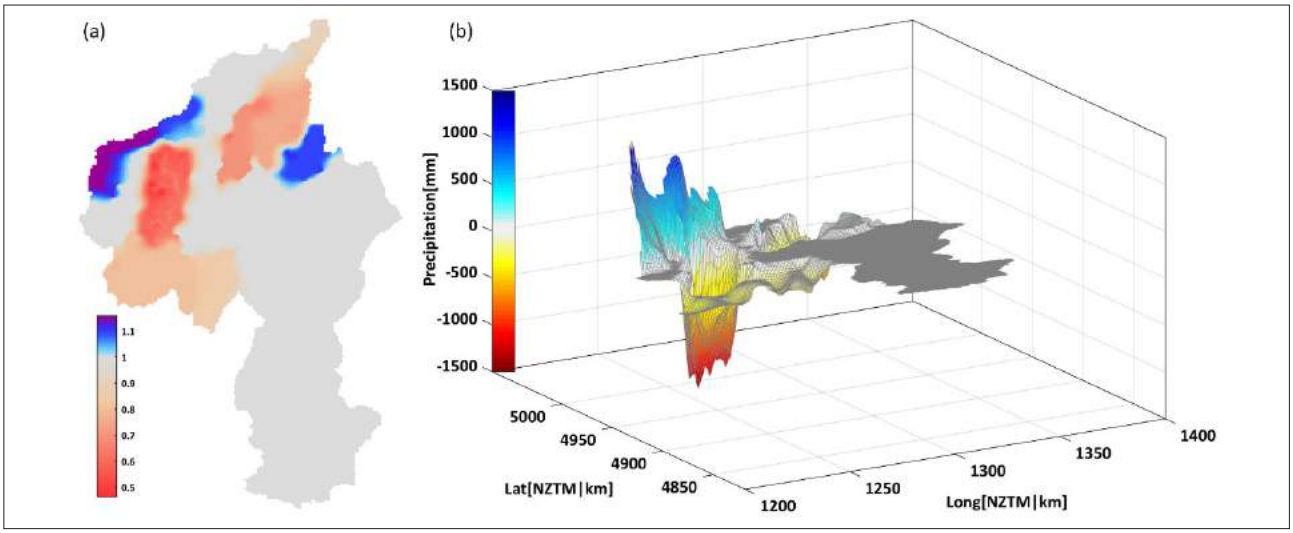

Figure 6: (a) The correction factor grid that was used to generate $SURF_{mod}$. (b) Difference between $SURF_{mod}$ and $SURF_{org}$.

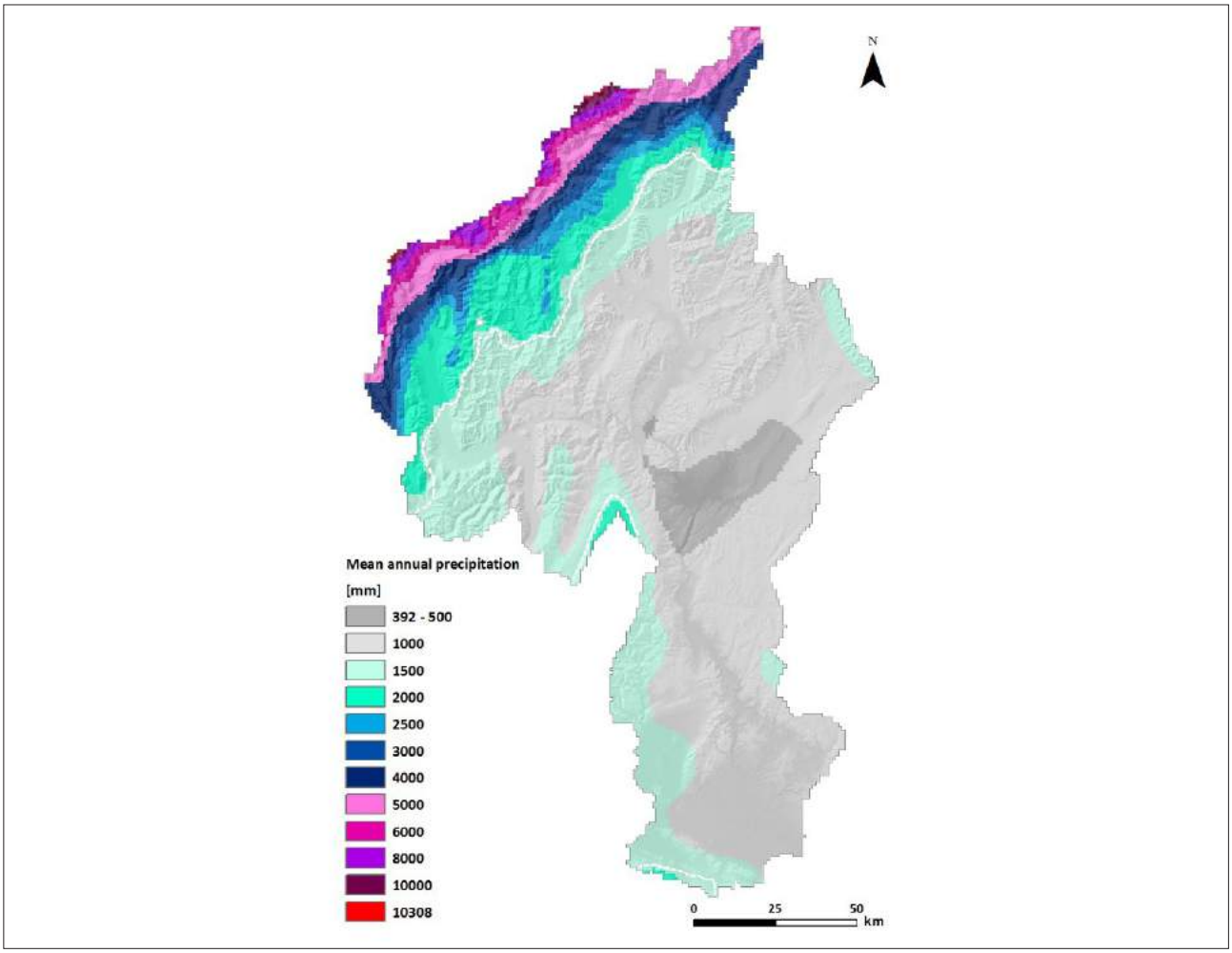

Figure 7: Mean annual (hydrological years) precipitation classes (mm) in the Clutha watershed based on the daily TS_{mod} fields. The dashed white line represents the 1415 mm isohyet, which corresponds to the mean precipitation of the catchment during that period.

Table 2: Mean annual precipitation in the Clutha catchment for hydrological years (1/4/1992 – 31/3/2012) based on VCSN and different versions of TS_{mod}: $SURF_{org}$ without ORC data and without undercatch correction, $SURF_{org}$ without ORC data and with undercatch correction, $SURF_{org}$ with ORC data and with undercatch correction, $SURF_{mod}$ with ORC data and with undercatch correction (= the complete approach).

Interpolation approach	Mean annual precipitation [mm]	Difference relative to VCSN [%]
VCSN (bilinear interpolation from ~5km to 1km)	1258	-
$SURF_{org}$_noORC_noUC	1370	8.9
$SURF_{org}$_noORC_UC	1428	13.5
$SURF_{org}$_ORC_UC	1484	18
$SURF_{mod}$_ORC_UC (=TS_{mod})	1415	12.5

found within that remaining zone. Finally, the annual water balance of the catchment is comprised of 1415 mm precipitation, of which 518 mm correspond to AET and 896 mm to streamflow (change in natural stores: 1 mm).

The effects of the various changes made with respect to the VCSN approach are shown in Figure 8 (see Table 2 for the mean catchment precipitation). When using $SURF_{org}$ in combination with the NIWA sites only and without undercatch correction annual precipitation is higher in most parts of the catchment (except in the north-eastern part) (Figure 8a). Adding the undercatch correction (Figure 8b) results in a moderate increase of precipitation (i.e. 4.2% overall change) with a similar pattern (compared to Figure 8a) of positive and negative differences across the catchment. Including the ORC sites substantially increases precipitation in the upper headwaters causing a predominantly positive difference that also extends into the north-western part of the catchment (Figure 8c). The effect of incorporating $SURF_{mod}$ (final component) is most apparent for the Shotover and Hawea sub-catchments (reduced precipitation up to 500-750 mm), and for the north-western headwaters (Figure 8d). Overall, the mean annual precipitation of the final product (i.e. TS_{mod}) is 12.5% higher compared to the VCSN (1258 mm) with positive differences exceeding 2000 mm towards the main divide.

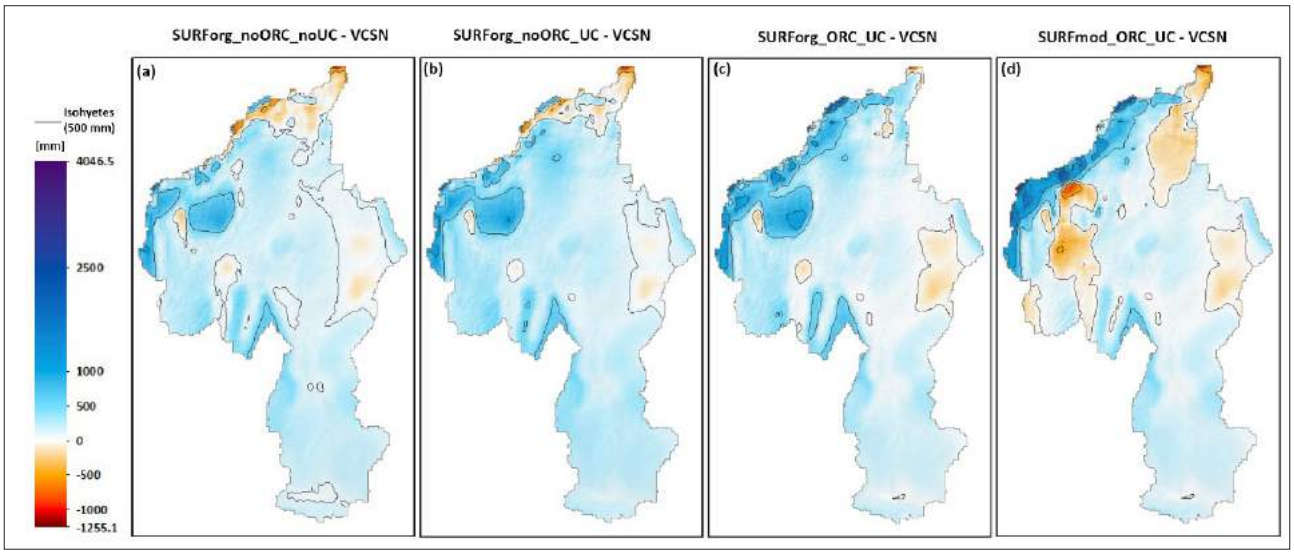

Figure 8: Differences between the mean annual precipitation of the VCSN and different versions of TS_{mod}: (a) $SURF_{org}$ without ORC data and without undercatch correction, (b) $SURF_{org}$ without ORC data and with undercatch correction, (c) $SURF_{org}$ with ORC data and with undercatch correction, (d) $SURF_{mod}$ with ORC data and with undercatch correction, i.e. the complete approach.

4. Discussion

The undercatch correction that was carried out before the interpolation of the station data was deemed necessary as undercatch is a known problem of point-based precipitation measurements that has been reported for many alpine regions (Yang et al., 1998; Mekis and Hogg, 1999). In the Pukaki basin with a comparable, albeit greater, precipitation gradient (710 – 13200 mm) the error induced by undercatch was estimated to range between 6 and 16% (Kerr et al., 2011). For the Clutha catchment as a whole the effect of undercatch correction was found to be smaller (i.e. 4.2%), but this value is expected to be higher for the upper Clutha where the terrain is more comparable to the alpine Pukaki catchment.

The technique that was used here to interpolate the undercatch corrected records follows up on existing studies that have used thin-plate spline interpolation for generating precipitation estimates in New Zealand (Tait et al., 2006; Sirguey, 2009). These studies showed that a TS with $SURF_{org}$ as a covariate resulted in the best accuracy and outperformed alternative approaches such as a bivariate spline or a trivariate spline with elevation as a covariate. In this study, $SURF_{org}$ was adjusted for some of the sub-catchments to allow for a realistic simulation of the water balance. The major modifications involved a reduction of orographic precipitation in the Shotover River, an increase of precipitation in the spillover zone of the Dart River and a decrease of precipitation in the remaining tributaries of Lake Wakatipu. Further adjustments were made by reducing precipitation in the Nevis and increasing precipitation in the upper Lindis. These modifications were considered justifiable as the construction of $SURF_{org}$ involved expert interpolation for locations where no observations were available (Tait et al., 2006). Using a water balance approach to estimate annual runoff across New Zealand, Woods et al. (2006) also found that an additional bias correction of the VCSN precipitation was necessary for several catchments to keep the model error below ±25% (including sub-catchments of the upper Clutha). In their study the error based on AET, precipitation and modelled streamflow was interpolated resulting in a smoothed bias surface which they used to correct their runoff estimates. The approach has also been adopted by Poyck et al. (2011) to model (i.e. TopNet) historical snow and streamflow processes in the Clutha catchment.

It should be noted that any potential errors associated with the term of AET would have introduced some uncertainty to the error assessment of modelled streamflow. Even though the uncertainty of modelled AET cannot be quantified, it is assumed to be relatively unimportant in the upper part of the Clutha where annual precipitation exceeds AET substantially. However, inaccuracies linked to modelled AET could be more important in the central parts of the catchment (i.e. Nevis and Lindis). Despite these uncertainties, the water balance modelling strongly suggested that the annual precipitation amounts of $SURF_{org}$ were inconsistent with the observed river flow of the affected sub-catchments between 1992 and 2012.

The differences between the two surfaces that were required to approximate the observed flow and hence the water balance suggest the following. First, precipitation in the north-western part of the Clutha is especially high, which could be explained by a particularly strong orographic uplift in this area and a resulting intensification in spillover precipitation. Second, the elevation of the terrain on the leeward side of the divide (i.e. the Shotover watershed) seems to have a substantially smaller effect on the precipitation intensity as suggested by $SURF_{org}$. The same applies (but to a lesser extent) for the Wakatipu sub-catchment where precipitation needed to be increased in the headwaters (error at The Hillocks of -5%) and decreased further eastwards (error at Frankton of +8%). The lack of rain gauges in the eastern parts of the Wakatipu basin means that $SURF_{org}$ in this area had to be based on expert knowledge, which could

explain the overestimation of precipitation here. Sirguey (2009) identified similar discrepancies for the Waitaki catchment, where $SURF_{org}$ showed substantial departures from the area weighted annual precipitation (as targeted by a 12-year water balance) in the sub-catchments Lake Pukaki (26%), Lake Ohau (-11%) and Lake Tekapo (-9%). Considering the dominance of the precipitation term (an order of magnitude greater than AET) and the extreme precipitation gradients of these catchments (e.g. the Waitaki and the Clutha) the use of flow records supplemented with estimates of AET (Sirguey, 2009) or modelled AET (Tait et al., 2006; this study) can thus be regarded as a useful approach to reduce errors in the precipitation term of a catchment.

While no precipitation data was available along the main divide of the Clutha watershed, Figure 2 suggests that the precipitation maximum is located somewhere between the sites at Young River and Milford Sound, which corresponds to 7 km east and 12 km west of the main divide, respectively. Hence a reasonably dense network of rain gauges upwind and downwind of the spill over zone is essential for capturing the actual distribution of precipitation across the Southern Alps. This highlights the importance of gauges located in the heavy precipitation area (i.e. Young River), where precipitation totals decrease dramatically over short horizontal distances.

As described in Tait et al. (2006) the use of $SURF_{org}$ outperformed the use of elevation as a covariate in the TS, which was shown by conducting a water balance validation. The remaining errors in the VCSN were still large for parts of the Southern Alps and ranged from -10 to -50% for the upper Clutha. The errors shown here when using $SURF_{org}$ were substantially lower for West Wanaka (-3%) and The Hillocks (-5%). As indicated by Figure 8c, including the ORC sites (Young River/P-O1 in particular) resulted in a substantial increase of precipitation in the headwaters of these sub-catchments which would have caused a substantial reduction of an otherwise comparable negative bias (with the VCSN). The undercatch correction would have also contributed to the bias reduction as shown in Figure 8b.

Tait et al. (2012) demonstrated that by including regional council data uncertainties in the VCSN product could be reduced (New Zealand wide: ~50% reduction of model error). However, due to data sharing difficulties between regional councils and the national climate database, the original VCSN (Tait et al., 2006) is still used as the operational product (Tait et al., 2012). Thus, based on the water balance validation conducted here the generated fields of daily precipitation constitute an improvement over the operational VCSN product as they offer a more realistic estimate on both the catchment and sub-catchment scale.

5. Conclusions

At a resolution of 1 km^2 the generated daily grids are considered to be representative estimates of the actual precipitation distribution inside the Clutha watershed. The fields allowed for a realistic simulation of the 1992-2012 water balance (model error within ±5% at all of the investigated sub-catchments) and can be considered as a valuable data source for environmental modelling studies focusing on the Clutha domain. The latter is highlighted by a recent hydrological modelling study in the Kawarau catchment where the TS_{mod} fields were successfully used to realistically model daily and monthly streamflow (Jobst et al., 2018). Future work could involve the use of a short term (≥ 1 year) flow network (not as prone to measurement errors as rain gauges) situated in the spillover zone of the catchment, which could help to further explore small scale errors in modelled precipitation inside the heavy rainfall zone. As mentioned by Tait et al. (2012), precipitation normal surfaces could also be specifically developed for certain synoptic patterns, which would allow improvements to be made in modelling precipitation distribution across the

complex terrain that characterises the Clutha catchment. Finally, a pragmatic way to incorporate the findings of this study into NIWA's operational VCSN dataset could be to update the original rainfall normal surface (inside the Clutha catchment) with the annual precipitation surface presented here.

Acknowledgements

The authors would like to thank Christian Zammit (NIWA) for the VCSN data and Pascal Sirguey (School of Surveying, University of Otago) for the implementation of the thin-plate spline. The meteorological data was kindly provided by NIWA, the Otago Regional Council and MetService. Streamflow records were provided by NIWA, Contact Energy Ltd. and the Otago Regional Council. This study was funded by a University of Otago Doctoral Scholarship to the lead author.

References

Anderton, P. W., 1974. Estimation of snow storage and melt in the catchment of Lake Pukaki. In: Proceedings of the New Zealand Hydrological Society Symposium, Otago University, Dunedin, New Zealand.

Chater, A. M. and Sturman, A. P., 1998. Atmospheric conditions influencing the spillover of rainfall to lee of the Southern Alps, New Zealand. International Journal of Climatology, Volume 18(1), pp. 77-92.

Chinn, T. J. 2001. Distribution of the glacial water resources of New Zealand. Journal of Hydrology New Zealand, Volume 40(2), pp. 139-187.

Cullen, N. J. and Conway, J. P., 2015. A 22 month record of surface meteorology and energy balance from the ablation zone of Brewster Glacier, New Zealand. Journal of Glaciology, Volume 61(229), pp. 931-946. doi: 10.3189/2015JoG15J004.

Fitzharris, B. B. and Garr, C. E. 1995. Simulation of past variability in seasonal snow in the Southern Alps, New Zealand. Annals of Glaciology, Volume 21, pp. 377-382.

Jobst, A. M., Kingston, D. G., Cullen, N. J., Sirguey, P. 2017. Combining thin-plate spline interpolation with a lapse rate model to produce daily air temperature estimates in a data-sparse alpine catchment. International Journal of Climatology, Volume 37, pp. 214-229. doi:10.1002/joc.4699.

Jobst, A. M., Kingston, D. G., Cullen, N. J., Schmid, J. 2018. Intercomparison of different uncertainty sources in hydrological climate change projections for an alpine catchment (upper Clutha River, New Zealand). Hydrology and Earth System Sciences, Volume 22, pp. 3125-3142. doi:10.5194/hess-22-3125-2018.

Kerr, T., Owens, I., Henderson, R. 2011. The precipitation distribution in the Lake Pukaki catchment. Journal of Hydrology New Zealand, Volume 50(2), pp. 361-382.

Lauscher, F. 1976. Weltweite Typen der Höhenabhängigkeit des Niederschlags. Wetter und Leben, Volume 28, pp. 80–90.

Marke, T., Mauser, W., Pfeiffer, A., Zängl, G. 2011. A pragmatic approach for the downscaling and bias correction of regional climate simulations: evaluation in hydrological modeling. Geoscientific Model Development, Volume 4(3), pp. 759-770. doi: 10.5194/gmd-4-759-2011.

McKerchar, A. I. and Pearson, C. P. 1997. Quality of long flow records for New Zealand rivers. Journal of Hydrology New Zealand, Volume 36(1), pp. 15-41.

Mekis, E., Hogg, W. D. 1999. Rehabilitation and analysis of Canadian daily precipitation time series. Atmosphere - Ocean, Volume 37(1), pp. 53-85.

Oudin, L., Perrin, C., Mathevet, T., Andréassian, V., Michel, C. 2006. Impact of biased and randomly corrupted inputs on the efficiency and the parameters of watershed models. Journal of Hydrology, Volume 320, pp. 62-83. doi: 10.1016/j.jhydrol.2005.07.016.

Poyck, S., Hendrikx, J., McMillan, H., Hreinsson, E. Ö., Woods, R. 2011. Combined snow and streamflow modelling to estimate impacts of climate change on

water resources in the Clutha River, New Zealand. Journal of Hydrology New Zealand, Volume 50(2), pp. 293-311. doi: 10.1007/s00704-012-0711-1.

Schönbrodt-Stitt, S., Bosch, A., Behrens, T., Hartmann, H., Shi, X., Scholten, T. 2013. Approximation and spatial regionalization of rainfall erosivity based on sparse data in a mountainous catchment of the Yangtze River in Central China. Environmental Science and Pollution Research, Volume 20(10), pp. 6917-6933. doi: 10.1007/s11356-012-1441-8.

Schulla, J. 2012. Model description WaSiM. Technical report. 324 pp. Available at http://wasim.ch

Sinclair, M. R., Wratt, D. S., Henderson, R. D., Gray, W. R. 1997. Factors affecting the distribution and spillover of precipitation in the Southern Alps of New Zealand—A Case Study. Journal of Applied Meteorology, Volume 36(5), pp. 428-442. doi:10.1175/1520-0450(1997)036<0428:FATDAS>2.0.CO;2.

Sirguey, P. 2009. Monitoring snow cover and modelling catchment discharge with remote sensing in the Upper Waitaki basin, New Zealand. Ph. D. thesis, School of Surveying, University of Otago, Dunedin, New Zealand. 436 pp.

Suprit, K., Shankar, D. 2008. Resolving orographic rainfall on the Indian west coast. International Journal of Climatology, Volume 28(5), pp. 643-657. doi: 10.1002/joc.1566.

Tait, A. B., Henderson, R., Turner, R., Zheng, X. 2006. Thin plate smoothing spline interpolation of daily rainfall for New Zealand using a climatological rainfall surface. International Journal of Climatology, Volume 26(14), pp. 2097-2115. doi: 10.1002/joc.1350.

Tait, A. B., Sturman, J., Clark, M. 2012. An assessment of the accuracy of interpolated daily rainfall for New Zealand. Journal of Hydrology New Zealand, Volume 51, pp. 25-44.

Woods, R., Hendrikx, J., Henderson, R., Tait, A. 2006. Estimating mean flow of New Zealand rivers. Journal of Hydrology New Zealand, Volume 45(2), pp. 95-110.

Wratt, D. S., Revell, M. J., Sinclair, M. R., Gray, W. R., Henderson, R. D., Chater, A. M. 2000. Relationships between air mass properties and mesoscale rainfall in New Zealand's Southern Alps. Atmospheric Research, Volume 52(4), pp. 261-282. doi: 10.1016/S0169-8095(99)00038-1.

Yang, D., Goodison, B. E., Ishida, S., Benson, C. S. 1998. Adjustment of daily precipitation data at 10 climate stations in Alaska: Application of World Meteorological Organization intercomparison results. Water Resources Research, Volume 34(2), pp. 241-256. doi: 10.1029/97wr02681.

Dobson spectrophotometer #17: past, present and future

S.E. Nichol

National Institute of Water and Atmospheric Research (NIWA), Private Bag 14901, Wellington, New Zealand

Correspondence: Sylvia.Nichol@niwa.co.nz

Key words: Dobson spectrophotometer, total ozone

Abstract

The Dobson spectrophotometer, which was developed in the late 1920s, measures atmospheric total column ozone. This paper presents the history of Dobson spectrophotometer #17 (D#17), which arrived in New Zealand in 1950. D#17 has been in operation at Kelburn in Wellington (1951 – 1970), Invercargill (1970 – 1987), and Arrival Heights in Antarctica (1988 - present). D#17's history includes a flooding, several overhauls, a semi-automation, and finally a complete automation. In the early days the main reasons for measuring total ozone were to develop an ozone climatology, and to investigate the relationship between ozone and the weather. From the mid-1970s the focus of ozone measurement largely changed to studying ozone trends (which includes Antarctic ozone depletion). This requires a traceable calibration history, which is discussed in detail. Plots of the D#17 total ozone record are provided.

1. Introduction

2018 marks 30 years of operation of Dobson spectrophotometer #17 (D#17) at the New Zealand atmospheric laboratory at Arrival Heights (77.83° S, 166.66° E; Figure 1) in Antarctica. But the history of D#17, and of ozone measurement in New Zealand, goes much further back in time than that. The Dobson spectrophotometer (Dobson, 1931), which was developed in the late 1920s by Dr G.M.B Dobson of Oxford University, is used to measure atmospheric total column ozone. The Dobson spectrophotometer is still widely regarded as being the standard instrument with which to measure atmospheric total column ozone from the ground. There are approximately 100 Dobson spectrophotometers currently operating around the world.

The Dobson spectrophotometer actually measures the relative intensity of solar radiation between selected wavelength pairs in the range of 300-350 nm. These measurements are then used to calculate the total amount of ozone between the instrument and the top of the atmosphere (i.e. total column ozone). The method of total ozone calculation can be found in Komhyr (1980). The units of measurement are Dobson Units (DU), with 100 DU being equivalent to a 1 mm thick slab of ozone at Standard Temperature and Pressure.

The precision of the Dobson spectrophotometer is considered to be ±1% (Evans et al., 2017). The accuracy of the instrument, which has been investigated by Basher (1982), is difficult to quantify as it depends on instrument-specific characteristics and observing conditions. Basher

Submitted: 12 October 2018
Accepted: 27 November 2018

(1982) estimates that under good operational conditions the accuracy is 3% or better.

2. Early ozone measurements in New Zealand

From the 1920s through to the 1960s the main reasons for measuring ozone were to develop an ozone climatology, and to investigate the relationship between ozone and the weather (Staehelin et al., 2018). New Zealand was involved in some early ozone measurements: a Féry quartz spectrograph was in operation at the Canterbury College in Christchurch, under the supervision of Dr C. Farr, from August 1928 to August 1929. The spectrograph was on loan from Dr Dobson, and was part of a "global" ozone monitoring network of five instruments (Dobson, 1930); the other instruments were in Switzerland, California, Egypt, and India. Dr Dobson invited local meteorologists to contribute short discussions on the relationships of daily ozone variations with meteorological conditions in their own regions. Dr E. Kidson, who was Director of the New Zealand Meteorological Service (NZMS), did this for the Christchurch measurements and his report is included in Appendix 2 of Dobson (1930).

3. Brief History of Dobson #17

Three prototypes of the Dobson spectrophotometer were made in the early 1930s. The first production run of 20 Dobson spectrophotometers was planned for 1936, at a cost of £385 each. Due to its involvement in the Christchurch ozone measurements, the NZMS was invited to place an order in this initial run and so avoid the higher costs for the instruments later on. The instruments were to be manufactured by R & J Beck Ltd of London, and the tests and calibration of the instruments were to be carried out by Dr Dobson at the Oxford ozone laboratory.

In 1937 the NZMS, which at that time was part of the Department of Scientific and Industrial Research (DSIR), gained approval to purchase a Dobson spectrophotometer, and so that is when the story of D#17 began. The order was placed by the DSIR, and the instrument was expected to arrive in New Zealand in 1938. However difficulties with calibrating the instrument, due to inclement weather at Oxford, significantly delayed its completion. In 1939, at the beginning of World War II, the New Zealand Government was approached to see if D#17, which still had not been dispatched to New Zealand, could be lent to the British Meteorological Office for the duration of the war to assist with "urgent defence investigations". The New Zealand Government agreed to that.

In 1947, after the end of the war, it was decided that D#17 would be overhauled and recalibrated before being sent to New Zealand. This work was done by Dr Dobson at Oxford. It took another two years for the replacement parts to be supplied, and D#17 was finally ready to be shipped to New Zealand at the end of 1949.

Figure 1: Map showing the location of the three sites where Dobson #17 has been operated (black). The other sites mentioned in this paper are shown in blue.

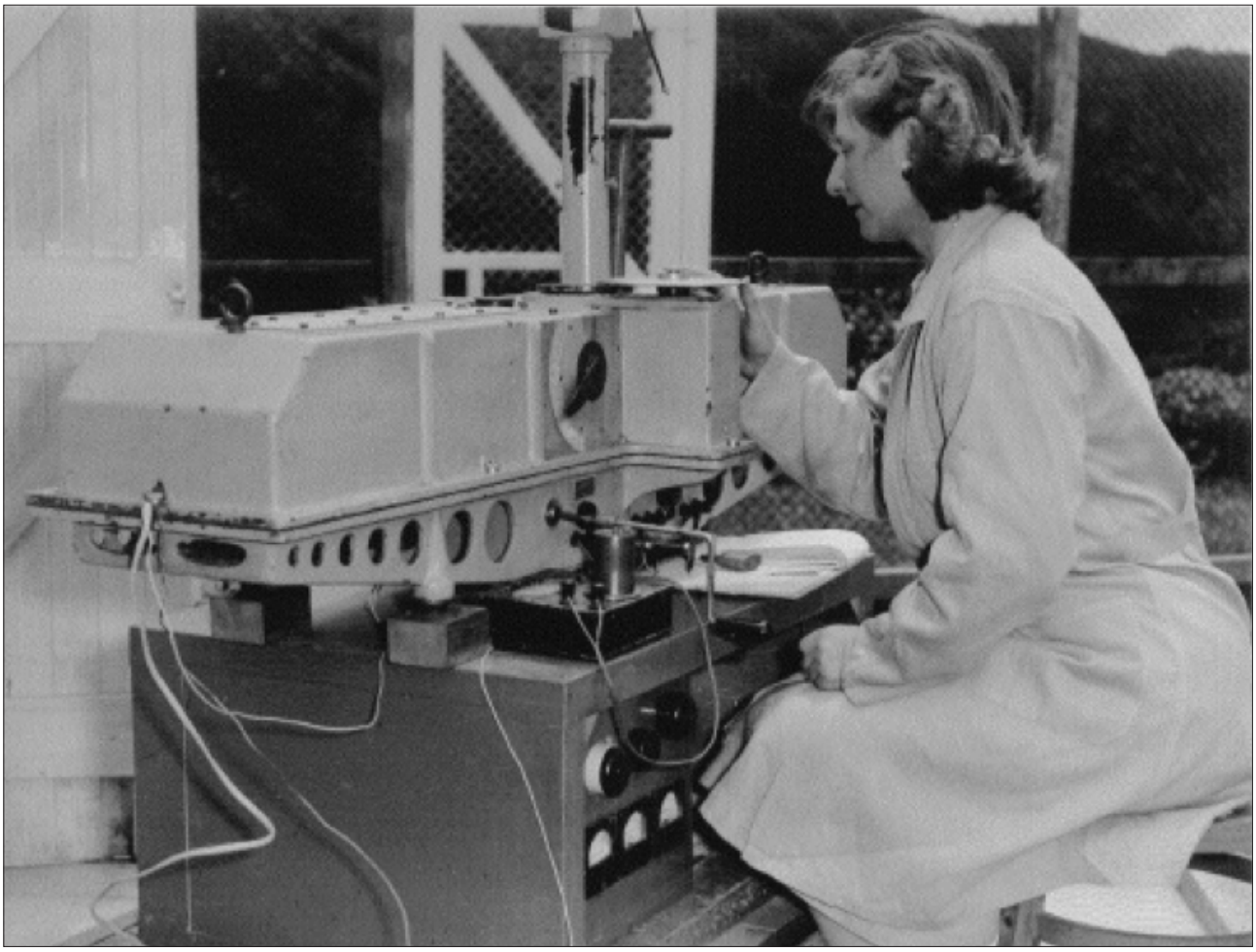

Figure 2: Edith Farkas operating Dobson #17 at Kelburn, about 1960.

So D#17 finally arrived in New Zealand in 1950, 13 years after the initial purchase. It was set up at the Dominion Physical Laboratory at Gracefield, Wellington, and some initial tests and ozone measurements were made there. By this time, the NZMS had become attached to the Air Department (de Lisle, 1986). So the ownership of D#17 was transferred from the DSIR to NZMS, and the instrument was set up at the NZMS office in Kelburn (41.28° S, 174.68° E; Figure 1), Wellington in July 1951.

The early measurements at Kelburn were performed by Elizabeth Porter, who tragically lost her life in December 1953 in the Tangiwai train disaster (https://iwonderweather.co.nz/story/women-in-weather/6388/keyword/women). The measurements continued at Kelburn, with increasing involvement from Edith Farkas (Figure 2) who had begun working for NZMS in 1953. This was her first scientific job in New Zealand, after arriving as a refugee from Hungary several years earlier (McGlone et al., 1990; https://iwonderweather.co.nz/story/women-in-weather/6388/keyword/women).

In 1962 the measurement programme was suspended due to the poor condition of D#17. The performance of the instrument had gradually deteriorated over time, until finally it became completely unserviceable. In 1963 it was decided to overhaul D#17, and resume the measurement programme for the International Quiet Sun Years (Pomerantz, 1963), which took place from January 1964 to December 1965. This overhaul was performed

Figure 3: Dobson #17 at Invercargill with (left to right) Tony Veitch, Bob Horridge, Edith Farkas, Dick Holloway, Mike Criglington (all NZMS); in late 1970s or early 1980s.

by the Commonwealth Scientific and Industrial Research Organisation (CSIRO) in Melbourne, Australia. Again there were major delays in obtaining replacement parts, and D#17 was finally back in operation at Kelburn in January 1965. Edith Farkas led the D#17 measurement programme from 1965 through to her retirement from NZMS in 1986.

D#17 remained in operation at Kelburn until June 1970, when it was moved to the NZMS Invercargill office (46.43° S, 168.35° E; Figure 3) which was at the airport. The move was made to help to fill in the latitudinal gap in the Australian network, which had Dobson spectrophotometers at Melbourne (37.67° S, 144.83° E) and Macquarie Island (54.50° S, 158.94° E).

In 1974 D#17's electronics were upgraded to Komhyr's (Komhyr and Grass, 1972) design. This involved replacing the amplifier, commutator, low voltage and high voltage power supplies with solid state components.

D#17 was badly damaged by floodwaters during the January 1984 Southland flood, when the Invercargill airport was flooded to a height of 2.5m (hwe.niwa.co.nz/event/January_1984_Southland_Flooding). D#17 required a complete overhaul to get it operational again, and so it was sent to the National Oceanic and Atmospheric Administration (NOAA) Dobson Laboratory in Boulder, Colorado, USA. During this rebuild, D#17's optical wedge was replaced with one of a more robust design (Evans et al., 2017). D#17 was back in service in Invercargill in June 1985.

In January 1987 another Dobson spectrophotometer was installed in New Zealand. Dobson #72 (D#72), which was part of the NOAA automated Dobson network, was installed at the DSIR station at Lauder (45.04°S, 169.68°E) in order to complement the other stratospheric measurements that were being made at the site. It made no sense to have New Zealand's two Dobsons operating in such close proximity to each other (Invercargill and Lauder are approximately 180 km apart). So NZMS conducted a review to decide where the best place to continue measurements with D#17 would be.

Figure 4: Dobson #17 at Arrival Heights after incorporation of the WinDobson software (February 2015), with (left to right) Kate McKenzie (Antarctica New Zealand), Sylvia Nichol (NIWA), Wills Dobson (NIWA), Koji Miyagawa (NOAA).

The Antarctic Ozone Hole had been discovered in 1985 (Farman et al., 1985; Chubachi, 1985), and so it was decided to move D#17 from Invercargill to the New Zealand Antarctic Research Programme (now known as Antarctica New Zealand) laboratory at Arrival Heights to contribute to investigations into Antarctic ozone depletion. Arrival Heights is very close to the American McMurdo station which, with the discovery of the Ozone Hole, had become a real hub for ozone depletion related measurements. There wasn't a Dobson operating in the McMurdo region, so the installation of D#17 at Arrival Heights in January 1988 was a welcome addition to the measurement programmes in the region. This included the ground-based measurements of nitrogen dioxide (an ozone depleting substance), which had been started by DSIR at Arrival Heights in 1982 (McKenzie and Johnston, 1982).

In 1992, the ownership of D#17 and operation of D#72 came under the one organisation when the National Institute of Atmospheric Research (NIWA) was formed as part of the reforms of the New Zealand government science sector. D#17 and D#72 are still in operation at Arrival Heights and Lauder respectively.

4. Changing methods of operation with Dobson #17

As already mentioned, the total ozone measurements are made by measuring solar ultraviolet radiation. When Dobson #17 was at Kelburn and Invercargill it was operated in the usual manner by storing it indoors and then wheeling it outside on a trolley to make the measurements, as shown in Figures 2 and 3. This method is not very suitable for Antarctic operation due to the

cold and windy conditions. A periscope system, using the design of Olafson (Komhyr, 1980; pers. comm. 1987), has been used for the Arrival Heights operation (Figure 4) so that Dobson #17 can be operated from within the laboratory. Also at Arrival Heights from April through to August the sun is too low in the sky to use sunlight to make the measurements, so during those months the measurements have been made using reflected moonlight instead.

Since D#17 has been in operation at Arrival Heights, it has undergone two significant instrument automations. In 2005 a digital encoder system, developed by NOAA (Evans, 2008), was incorporated into the instrument which semi-automated the data collection. Up until this point the whole measurement process was basically the same as it had been for the preceding 65 years, with measurement times and instrument dial readings being written down by hand onto measurement log sheets. In the very early days, the calculations to derive the total ozone values were done by hand, using these hand-recoded values and various look-up tables (Komhyr, 1980). In later years these calculations were performed using computers with the hand-recorded values being transcribed into input files. The 2005 automation resulted in the measurement times and instrument dial readings being recorded directly into computer input files by the digital encoder system.

The second automation of D#17, which took from November 2014 to January 2015 to complete, incorporated automation controls directly into the instrument so that the measurements are now driven by the automated WinDobson software. D#72 has been running the WinDobson software since 2012.

The WinDobson package (Miyagawa, 1996), which was developed by the Japan Meteorological Agency, provides a standardized approach to operation, quality assurance and data analysis of Dobson observations. The WinDobson automation provides more consistent results from consecutive measurements. This standardized measurement approach is particularly useful at a station like Arrival Heights, where the instrument operators change annually; more than 60 operators have worked with D#17 over its 30 years of operation at Arrival Heights.

5. Dobson #17 measurements

The calibration history of D#17, from 1965 through to 1987, is summarised in Farkas (1989), and presented in more detail in Nichol and Coulmann (1990). Both Farkas (1989) and Nichol and Coulmann (1990) restricted their analysis to data from 1965 onwards i.e. the period after the overhaul of D#17 by CSIRO in 1963/1964. As part of the 1963/1964 overhaul, D#17 was compared directly with Regional Standard Dobson #105. These instrument comparisons are a method of transferring calibrations from one instrument, usually a well-calibrated Regional Standard, to another instrument (Komhyr, 1980). They provide traceability to the world standard, and thereby improve consistency of measurement across the world network. No such comparisons had been carried out during the period 1950 to 1962, and so the D#17 data for that period were excluded from the Farkas (1989) and Nichol and Coulmann (1990) analyses.

As ozone research became more oriented towards the analysis of long term behaviour, there were increased international efforts to ensure good instrument calibration status and standardisation of measurement techniques, so instrument comparisons became much more frequent. D#17 was compared with Regional Standard Dobsons in Australia in 1978, and in Canada in 1981. D#17 was compared with the World Standard Dobson in Boulder, Colorado in 1985, after it had been overhauled. Since 1991, D#17 has been compared with the Regional Standard Dobson in Australia at approximately 5-yearly intervals.

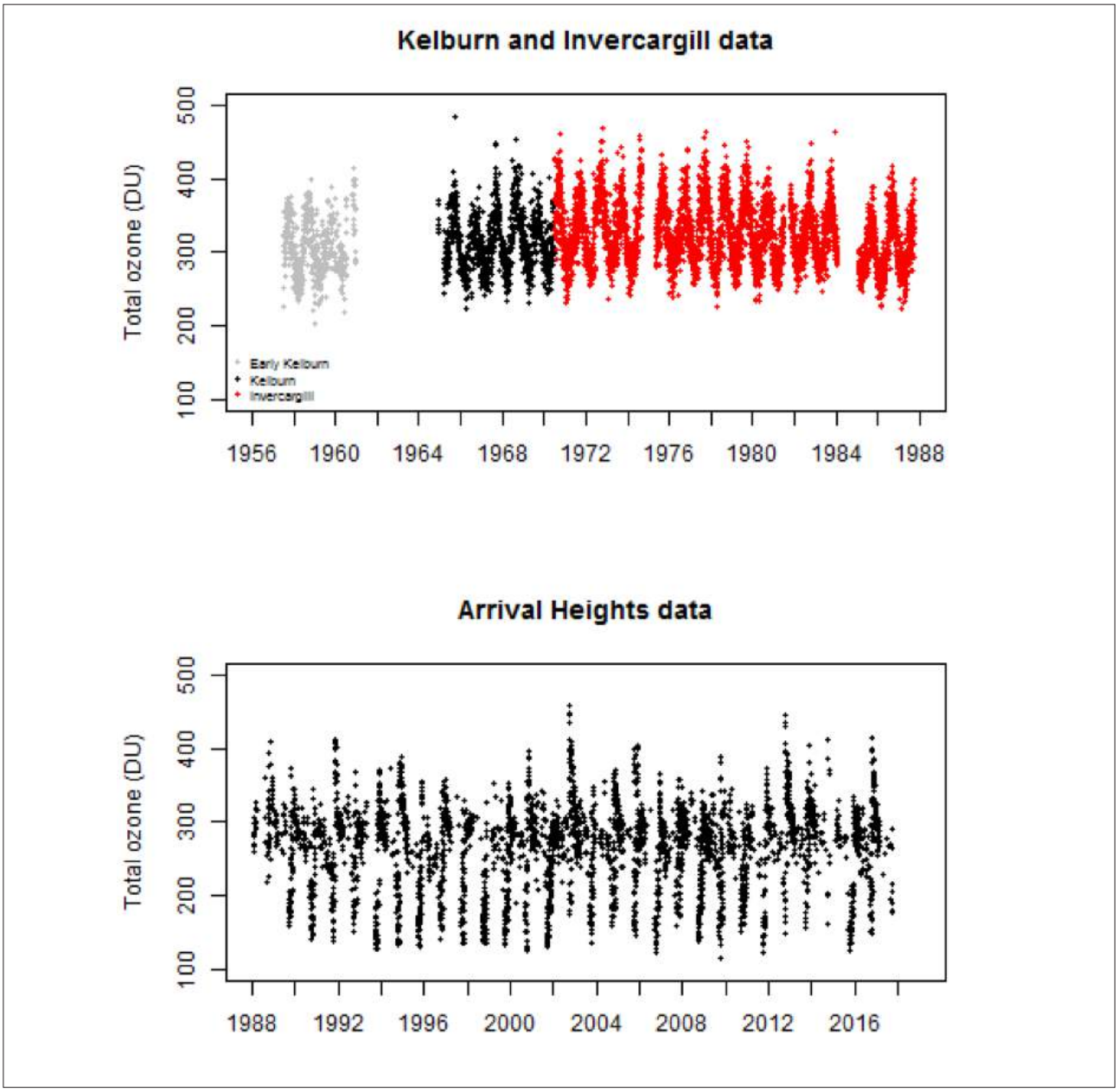

Figure 5: Daily total ozone data from Dobson #17 for Kelburn (grey and black, top panel), Invercargill (red, top panel) and Arrival Heights (bottom panel). NB the Kelburn data from 1957-1960 (in grey, top panel)) are included but they are not considered to be well-calibrated data.

Figure 5 shows the D#17 measurements from 1957 to 2017. Although the data from 1957 to 1961 are not well calibrated data, they have been included in Figure 5 for the sake of completeness. There is a 1-year gap in the Invercargill record from February 1984 through to February 1985, which was caused by the flood damage to D#17. Nichol and Coulmann (1990) found D#17 to be well calibrated on both sides of the data gap. The Kelburn (1957-June 1970) and Invercargill (June 1970-1987) data show typical mid-latitude behaviour with a seasonal minimum in late summer/early autumn, with values around 280 Dobson Units (DU), and seasonal maximum in springtime, with values around 370 DU.

The Arrival Heights data (Figure 5) show a seasonal pattern with a minimum in September or October, which

is due to the Ozone Hole. The seasonal maximum occurs in late November or early December, when the Ozone Hole breaks up. The lowest ozone value recorded at Arrival Heights with D#17 is 115 DU (on 29 September 2009).

The D#17 data are available from the World Ozone and Ultraviolet Data Centre (https://woudc.org/) and the Network for the Detection of Atmospheric Composition Change (http://www.ndsc.ncep.noaa.gov/data/).

6. Changing focus of ozone research

From the mid-1970s, when the possible link between ozone depletion and increasing chlorine in the atmosphere was first put forward (Molina and Rowland, 1975), the focus of ozone measurement largely changed to studying ozone trends. The first real evidence of ozone depletion came with the discovery of the so-called Antarctic Ozone Hole (Farman et al., 1985; Chubachi, 1985). The first reported Antarctic Ozone Hole measurements were from the Dobson spectrophotometer at Syowa (69.00° S, 39.58° E) station, where values dropped to about 210 DU during October 1982 (Chubachi, 1985). The significance of those measurements, which were presented at the Ozone Commission Symposium in Halkidiki in 1984, was not fully recognized at the time. Farman et al. (1985) presented measurements from the Dobson spectrophotometers at Halley Bay (75.61° S, 26.20° W) and Argentine Islands (65.25° S, 64.27° W) stations for the period 1957 through to 1984. Those measurements clearly showed that the October total ozone values for the period 1980-1984 were much lower than for the period 1957-1973.

A later study, using ozone measurements made by satellites, showed a decrease in total column ozone on a global scale (Stolarski et al., 1991). Data from the Dobson network also indicated that the total column ozone had decreased on a global scale since 1979 (McPeters and Komhyr, 1991), although to a lesser extent than suggested by the satellite data. Analysis of the Invercargill measurements (Farkas, 1989; Nichol and Coulmann, 1990) show a decrease of about 0.8% per year from 1980 to 1987, which is very similar to that reported for the Australian Dobson stations (Atkinson and Easson, 1989) over the same period.

The study of ozone trends requires good quality ozone time series, preferably extending back in time over decades, and thus builds on the hard work of numerous researchers over many years. The importance of the work by the early researchers was not always fully recognised at the time, as for example is indicated in the acknowledgements in Stolarski et al. (1991): "We would also like to thank Arlin Krueger, the Principal Investigator for TOMS, who persisted for many years when nobody cared about the TOMS data".

In 1988, the World Meteorological Organisation (WMO) recognised 26 ozone researchers for the major contribution they had made to ozone research over the preceding 30 years (Bojkov and Fabian, 1989). One of those recognised was Edith Farkas who, as already mentioned, worked with D#17 from the mid-1950s through to her retirement from NZMS in 1986. Over that time she established a regular and reliable ozone measurement programme with D#17, and produced many publications. She published the first measurements from D#17 (Farkas, 1954 and 1958), and her last publication (Farkas, 1989), which analysed the Kelburn and Invercargill total ozone measurements for the period 1965 to 1987, was published after her retirement from NZMS.

7. The Montreal Protocol

As already stated, in the mid-1970s it was postulated that there was a link between ozone depletion and increasing chlorine in the atmosphere (Molina and Rowland, 1975). International concern about the ozone layer increased over time, and resulted in the signing of the Vienna

Convention on the Protection of the Ozone Layer in 1985. This was an agreement to do something about ozone depletion. It set up the framework which led to the Montreal Protocol, which set targets for reducing the production and consumption of ozone depleting substances. The Montreal Protocol was signed in 1987 and it came into effect in 1988. As a result, atmospheric concentrations of ozone depleting substances reached a maximum in the late 1990s, and have been declining since then (Staehelin et al., 2018)

Ozone measurements, including those from the Dobson network, feed into the WMO/United Nations Environmental Program Scientific Assessments of Ozone Depletion (e.g. WMO, 2014), which measure the success of the Montreal Protocol. We intend to keep D#17 operating at Arrival Heights to monitor Ozone Hole developments. The D#17 measurements have been used in modelling studies (Bodeker et al., 2001; Nichol et al., 2003; Oman and Douglass, 2014; Fogt and Zbacnik, 2014) and satellite validation studies (Wood et al, 2002; Bramstedt et al., 2003; Kuttippurath et al., 2018).

Acknowledgements

D#17 has been in operation in New Zealand (and territories) for nearly 70 years. There have been at least 100 people who have worked with the instrument over that time, which is too many to name individually, and also the names of many of those involved in the early years are unknown to us. However we would like to acknowledge those that we do know about. First and foremost, we sincerely thank Edith Farkas for her great work and commitment in establishing a reliable measurement programme. Many of the details about the early operations with D#17 come from her notes. Thanks are also due to the staff at the NZMS Invercargill office, including Dick Holloway and Keith Herrick. The measurements at Arrival Heights have been very well supported by Antarctica New Zealand with logistical and technical support (involving at least 60 operators). Tom Clarkson and Stephen Wood (NIWA) also contributed to the Arrival Heights operation. There are also many international collaborators who have worked with D#17; in recent times they have been: Bob Grass and Walter Komhyr (NOAA) for the 1984 overhaul; Jim Easson and Steve Rhodes (Australian Bureau of Meteorology) for Dobson inter-comparisons; Bob Evans and Koji Miyagawa (NOAA) for the instrument automations.

References

Atkinson, R. J.; Easson, J. R., 1989. Re-evaluation of the Australian total ozone data record. Proceedings of the Quadrennial Ozone Symposium and Tropospheric Ozone workshop, held in Gottingen, Federal Republic of Germany, 4-13 August 1988. Edited by Bojkov and Fabian. A Deepak Publishing, Virginia, USA.

Basher, R. E., 1982. Review of the Dobson spectrophotometer and its accuracy, WMO Global Ozone Research and Monitoring Project Report No 13, Geneva.

Bodeker, G. E.; Scott, J. C.; Kreher, K.; McKenzie, R. L., 2001. Global ozone trends in potential vorticity coordinates using TOMS and GOME intercompared against the Dobson network: 1978–1998. J. Geophys Res., 106, 23029-23042, https://doi.org/10.1029/2001JD900220.

Bojkov, R. D.; Fabian, P., 1989. Ozone in the atmosphere. Proceedings of the Quadrennial Ozone Symposium and Tropospheric Ozone workshop, held in Gottingen, Federal Republic of Germany, 4-13 August 1988. Edited by Bojkov and Fabian. A Deepak Publishing, Virginia, USA.

Bramstedt, K.; Gleason, J.; Loyola, D.; Thomas, W.; Bracher, A.; Weber, M.; and Burrows, J. P., 2003. Comparison of total ozone from the satellite instruments GOME and TOMS with measurements from the Dobson network 1996–2000, Atmos. Chem. Phys., 3, 1409-1419, https://doi.org/10.5194/acp-3-1409-2003.

Chubachi S., 1985. A Special Ozone Observation at Syowa Station, Antarctica from February 1982 to January 1983. In: Zerefos C.S., Ghazi A. (eds) Atmospheric Ozone. Springer, Dordrecht. https://doi.org/10.1007/978-94-009-5313-0_58.

De Lisle, J. F., 1989. Sails to Satellites: a history of meteorology in New Zealand. New Zealand Meteorological Service, Wellington, New Zealand.

Dobson, G. M. B., 1930. Observations of the Amount of Ozone in the Earth's Atmosphere, and its Relation to other Geophysical Conditions – Part IV. Proceedings of the Royal Society A, 129, 411-433, doi:10.1098/rspa.1930.0165.

Dobson, G. M. B., 1931. A photoelectric spectrophotometer for measuring the amount of atmospheric ozone. P. Phys. Soc., 43, 324–339, https://doi.org/10.1088/0959-5309/43/3/308.

Evans, R. D.; Komhyr, W. D., 2008. Operations Handbook – Ozone Observations with a Dobson Spectrophotometer. World Meteorological Organization Global Atmosphere Watch GAW No.183, WMO/TD-No. 1469.

Evans, R. D.; Petropavlovskikh, I.; McClure-Begley, A.; McConville, G.; Quincy, D.; Miyagawa, K., 2017. Technical note: The US Dobson station network data record prior to 2015, re-evaluation of NDACC and WOUDC archived records with WinDobson processing software. Atmos. Chem. Phys. 17, 12051-12070, doi 10.5194/acp-17-12051-2017.

Farkas, E., 1954. Measurements of atmospheric ozone at Wellington, New Zealand. New Zealand Meteorological Service Technical Note 114.

Farkas, E., 1958. Measurements of atmospheric ozone at Wellington, New Zealand. Addendum to New Zealand Meteorological Service Technical Note 114.

Farkas, E., 1989. Long term variations and recent negative anomalies of New Zealand total ozone and Umkehr vertical ozone distributions. Proceedings of the Quadrennial Ozone Symposium and Tropospheric Ozone Workshop, held in Gottingen, Federal Republic of Germany, 4-13 August 1988. Edited by Bojkov and Fabian. A Deepak Publishing, Virginia, USA.

Farman, J. C.; Gardiner, B. G.; Shanklin J. D., 1985. Large losses of ozone in Antarctica reveal seasonal ClOx/NOx interaction. Nature, 315, 207-210.

Fogt, Ryan L.; Zbacnik, Elizabeth A., 2014. Sensitivity of the Amundsen Sea low to stratospheric ozone depletion. Journal of Climate, 27, 9383-9400.

Komhyr, W. D.; Grass, R. D., 1972. Dobson spectrophotometer modification. J Appl. Met. 11, 858-863.

Komhyr, W. D., 1980. Operations handbook – ozone observations with a Dobson spectrophotometer. WMO Global Ozone Research and Monitoring Project Report 6, Geneva.

Kuttippurath, J.; Kumar, P.; Nair, P. J.; Chakraborty, A., 2018. Accuracy of satellite total column ozone measurements in polar vortex conditions: Comparison with ground-based observations in 1979–2013. Remote Sensing of Environment, 209, 648-659.

McGlone, M.; Clarkson, T.; Fitzharris, B., 1990. Unsettled Outlook – New Zealand in a greenhouse world, GP Books, Wellington, New Zealand.

McKenzie, R. L., and Johnston, P. V., 1984. Springtime stratospheric NO2 in Antarctica. Geophysical Research Letters, 11, 73-75, doi:10.1029/GL011i001p00073, 1984.

McPeters, R. D.; Komhyr W. D., 1991. Long-term changes in SBUV/TOMS relative to World Primary Standard Dobson Spectrometer 83. J. Geophys Res., 96, 2987-2994.

Miyagawa, K., 1996. Development of automated measuring system for Dobson ozone spectrophotometer. Atmospheric Ozone: Proceedings of the XVIII Quadrennial Ozone Symposium L'Aquila, Italy, 12–21 September 1996, Parco Scientifico e Tecnologici d'Abruzzo, L'Aquila, Italy, vol. 2, 951–954.

Molina, M. J.; Rowland, F. S., 1974. Stratospheric sink for

chlorofluoromethanes: Chlorine atom-catalysed destruction of ozone. Nature. 249 (5460): 810, doi:10.1038/249810a0.

Nichol, S.; Coulmann, S., 1990. New Zealand ozone database review. NZMS Report.

Nichol, S.E.; Pfister, G.; Bodeker, G.E.; McKenzie, R.L.; Wood, S.W.; Bernhard, G., 2003. Mitigation of cloud reduction of UV in the Antarctic due to high surface albedo. Journal of Applied Meteorology, Vol 42, No. 8, 1174-1183.

Oman, Luke D.; Douglass, Anne R., 2014. Improvements in total column ozone in GEOSCCM and comparisons with a new ozone-depleting substances scenario. J. Geophys Res., 119, 5613-5624.

Pomerantz, M. A., 1963. International Years of the Quiet Sun, 1964-65. Science 142, 1136-1143, doi: 10.1126/science.142.3596.1136

Staehelin, J.; Viatte, P.; Stübi, R.; Tummon, F.; Peter, T., 2018. Stratospheric ozone measurements at Arosa (Switzerland): history and scientific relevance. Atmos. Chem. Phys. 18, 6567-6584, doi 10.514/acp-18-6567-2018.

Stolarski, R. S.; Bloomfield, P.; McPeters, R. D.; Herman, J. R., 1991. Total ozone trends deduced from Nimbus 7 TOMS data. Geophysical Research Letters 18, 1015.

WMO, 2014. Scientific Assessment of Ozone Depletion: 2014, Global Ozone Research and Monitoring Project, Geneva, Switzerland, Report No. 55.

Wood, S.W.; Bodeker, G.E.; Boyd, I.S.; Connor, B.J., Johnston, P.V.; Matthews, W.A.; Nichol, S.E.; Murcray, F.J.; Nakajima, H.; Sasano, Y., 2002. Validation of version 5.20 ILAS HNO3, CH4, N2O, O3, and NO2 using ground-based measurements at Arrival Heights and Kiruna. J. Geophys. Res., 107, 8208, doi:10.1029/2001JD000581.

Stability of solar radiation sensor calibration in the NZ Climate Network

J. B. Liley [1]

[1] *National Institute of Water & Atmospheric Research, PO Box 50061 Omakau 9352*

Correspondence: Ben.Liley@niwa.co.nz

Key words: pyranometers, solar radiation, NZ climate database, calibration

Abstract

The NIWA Climate Database holds solar radiant energy data for ~150 stations around New Zealand and the southwest Pacific, largely from Licor photodiode sensors but with Eppley PSPs at some sites. There are good multi-year data for about 70 sites, including all major population centres. There are hourly global, diffuse, and direct radiation data from Eppley sensors at Kaitaia, Paraparaumu, and Invercargill since 1988, but the best NZ solar radiation data are from the Baseline Surface Radiation Network (BSRN) station at Lauder, in Central Otago. Meteorological Service of New Zealand Limited (MetService) has regularly calibrated their own and other solar radiation sensors, at Paraparaumu, for the New Zealand Climate Network but since November 2013 NIWA's instruments have been calibrated at Lauder. Instruments that remain in statistical control are redeployed to the next vacant site, but the practice of using the new calibration directly has led to dubious steps in the data. Records of calibrations and deployments are incomplete, and somewhat error-prone, but they show that dividing out applied calibrations actually reduces the variance in (near-to-) clear-sky values. For more reliable time series for analysis of patterns or trends, regular calibration should be combined with statistical control theory, so that instrument response that can be regarded as constant or slowly trending does not become an additional source of error.

1. Introduction

Global irradiance, the solar energy flux through a horizontal surface, is a critical parameter in Earth's energy balance, in the energy flux of weather and climate systems, as a driver of the biosphere, and increasingly for renewable energy supply. Detecting changes in global energy balance requires data of very high quality, motivating formation in the 1990s of the global Baseline Surface Radiation Network (Ohmura et al., 1998). For the 48 open and 11 closed BSRN stations, the direct and diffuse components of solar radiation are or were measured with solar tracking pyrheliometers and shaded pyranometers to the highest available accuracy and high time resolution (1 to 3 minutes). The data are widely used in analyses of global energy balance and validation of satellite-derived data and earth system models.

New Zealand's only BSRN station is at the Lauder site of the National Institute of Water & Atmospheric Research Ltd. (NIWA), with BSRN data since 1999. Direct and diffuse radiation were measured by the NZ

Submitted: 12 October 2018
Accepted: 28 November 2018

Meteorological Service and subsequent MetService at Kaitaia, Paraparaumu, and Invercargill from the late 1980s with tracking pyrheliometers and a pyranometer with shade band, logged at hourly intervals. From 2000 the instruments were transferred to NIWA data loggers, with both hourly and 10-minute recording. In 2011, trackers were upgraded to EKO systems using a shade ball for diffuse measurements.

The New Zealand National Climate Database (CLIDB), managed by NIWA and accessible at https://cliflo.niwa.co.nz/, holds global irradiance data for over 200 climate stations around New Zealand. Of those stations, 181 are open, and 100 have at least 10 years of data. Most of the stations are operated by NIWA, 48 belong to MetService, and some are owned by other CRIs, Airways Corporation, regional and district councils, universities, and others.

The New Zealand global irradiance data find use in calculating solar heating, evaporation rates, plant growth, and the like. Within NIWA, they have been used to develop maps of solar flux (Tait and Liley 2009), to estimate UV radiation anywhere in the country (Bodeker and McKenzie 1996; Bodeker et al., 2002; Bodeker et al., 2006), and to calculate available solar energy on a panel of arbitrary tilt and bearing allowing for horizon shading (http:/solarview.niwa.co.nz). All of these NIWA products use the ratio of measured global irradiance to clear sky values, and that calculation raises a question about the stability of instrument calibration.

MetService operates a calibration facility at Paraparaumu, and all pyranometers in the New Zealand climate network were previously calibrated there. Since November 2013, NIWA sensors have been calibrated at Lauder. Only 17 of the NIWA pyranometers are thermopile radiometers (all Eppley) that measure the 300 nm to 2800 nm integral (e.g., https://s.campbellsci.com/documents/au/manuals/psp.pdf). The manufacturer suggests figures of 2% uncertainty in hourly and 1% in daily integrals (unstated, but presumably both 2σ) for these instruments, while the calibration certificates from the MetService's Calibration Laboratory give a figure, including reference sensor uncertainty of ±2.8% (2σ), of ±6% (2σ) in hourly data. Most of the other sensors are Licor silicon photodiodes, for which the manufacturer suggests a calibration uncertainty of ±3% within 60° angle of incidence (https://www.licor.com/env/products/light/pyranometer.html). MetService calibration certificates give a figure of ±8% (2σ) for hourly values in field data.

The response of silicon sensors drops sharply from 1000 to 1100 nm and beyond, so the calibration against reference thermopile pyranometers is applicable only to the extent that the overall spectrum in field measurement is similar to that at calibration.

For most meteorological and climate parameters, such as temperature, pressure, humidity, or wind speed, the reliability of time series depends on periodic calibration of sensor response against reference sensors or collocated instruments. Drifting instrumental response may be suspected, and detectable in the calibration record, but it cannot usually be inferred just from field data with a single instrument.

With solar radiation data, a further test arises naturally for checking both stability and absolute response when the aerosol optical depth is low. As demonstrated below, fitting the diurnal variation with a suitable model to detect days with clear sky (minimal cloud) provides a 'field calibration' or verification method that readily detects any major errors in response or alignment. Here I compare the results of such analysis with the formal calibration record.

2. Data

Radiation data in CLIDB are primarily stored at hourly resolution, and are available free from http://cliflo.niwa.

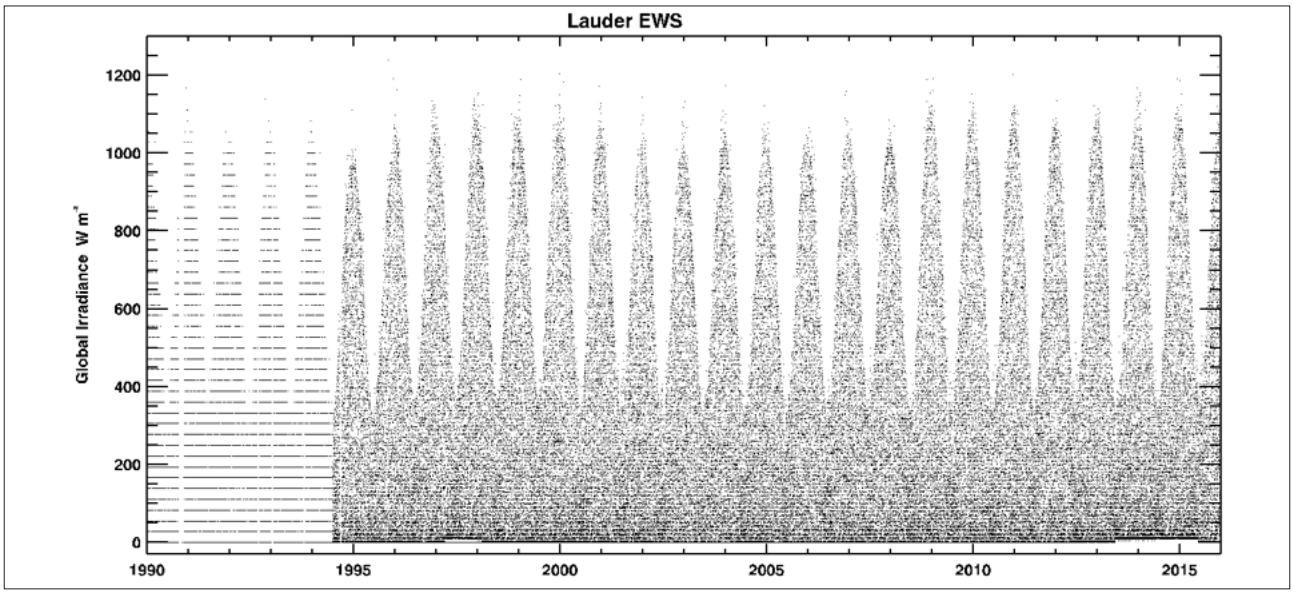

Figure 1: Time series of hourly-mean global irradiance measurements at the Lauder EWS (CliFlo #5535, 45.040° S, 169.684° E, 375 masl).

co.nz, or on request to cliflo@niwa.co.nz for specific datasets. From an error when CLIDB was established, the data were stored at degraded resolution. They were expressed just to one decimal place in units of MJ m^{-2}, for which hourly values range up to at most 4.5, and median daytime values are around 1 MJ m^{-2}. The mistake was discovered during development of the NIWA UV Atlas (Bodeker and McKenzie 1996), and some earlier data at better resolution were recovered, but mostly only data from 1995 onward are useful for analysis here. An example dataset is shown in Figure 1.

The calibration factors of all the radiation sensors used by NIWA have been maintained in a spreadsheet by NIWA's Instrument Systems staff (Andrew Harper, personal communication). It records just month and year when each sensor was deployed at a given station, and the month and year when it was calibrated. It might be helpful to have higher precision in those dates, especially of field deployment, but it has little effect on the analysis here.

Data from 90 NIWA Electronic Weather Stations (EWS) and Compact Weather Stations (CWS) were used for the initial analysis. It could readily be extended to the Automatic Weather Stations (AWS) operated by MetService and others, if corresponding calibration records are available.

For detailed study I focus on data from the Lauder EWS site, which allow comparison with data from the BSRN instruments on the Lauder Optics building 200m to the west. The latter data are available from the BSRN website at https://bsrn.awi.de/data/data-retrieval-via-pangaea/. The BSRN instrumentation at Lauder comprises Kipp & Zonen CMP21 pyranometers, a CHP1 pyrheliometer (direct normal incidence pyranometer), and a CAL17 pyrgeometer (global infrared irradiance), with the pyrheliometer and shade disks for the diffuse pyranometer and pyrgeometer mounted on a Middleton Solar tracker (Forgan 2009). The data are processed by the Australian Bureau of Meteorology to the stringent standards of the BSRN (Ohmura et al. 1998), logging data at 1 Hz and recording statistics at 1-minute resolution, with consistency checks.

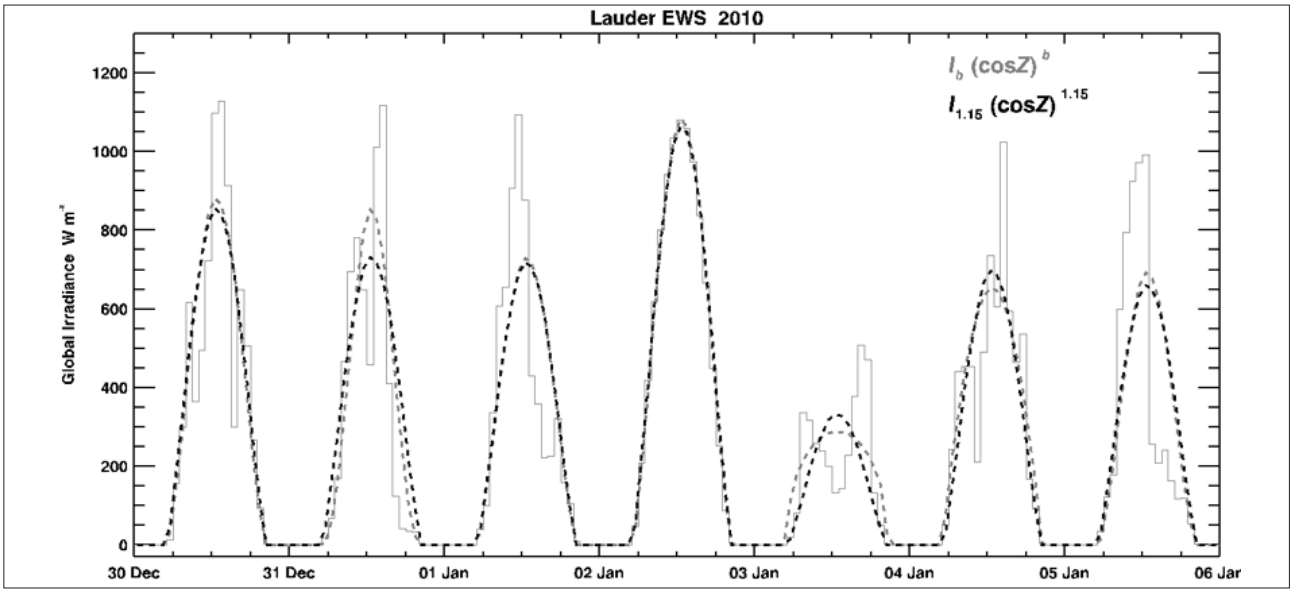

Figure 2: Lauder EWS hourly global irradiance data (light grey, stepped) for the beginning of 2010, showing fitted clear-sky models for variable (dashed, grey) or fixed (dashed, black) exponent b.

3. Analysis

The calibration-constancy of global irradiance data is best examined by consideration of clear-sky days, which are readily apparent in plots of diurnal variation. Such days can be detected algorithmically as follows.

For all 90 of the selected NIWA stations, hourly global irradiance data for each day of their respective time-series were fitted with a function of the form

$$I = I_b \cos(Z)^b \qquad (1)$$

where I is the predicted irradiance, Z is solar zenith angle, b is a fitted constant, and I_b is a fitted constant giving the irradiance for overhead sun.

An example is shown in Figure 2, with the lighter grey curve indicating the function for variable exponent b.

Although such fitting can be achieved by regression of log(I) on log(cos$Z$), that is unduly sensitive to small values and requires appropriate weighting. Instead, the non-linear fitting used here assumes constant variance in additive residuals (homoscedasticity). That assumption is imperfect, because there are no negative values, as would be implied by symmetry in the residual error for very low solar elevation.

Figure 2 suggests that the clear days can be selected as those with the largest values of I_b, but there is substantial covariance (r = 0.675 for N = 121,520 site-days in the data used here) between b and I_b (not shown). Using a prescribed value of $b = \beta$ avoids this problem, and it also means that the model can be fitted just with linear regression of I on $(\cos Z)^\beta$. That is sufficiently quick, even for the 394,743 site-days in the full dataset, to permit some exploration of the best value.

The selected value of b = 1.15 has previously been found to fit very well with 1-minute data for the clearest days in the BSRN dataset, and it remains a good fit as they are aggregated to hourly values like the CliDB data. It is below the mean (1.33) of the fitted b values for days selected as reasonably clear (see below), but within one standard deviation (0.22). It lies between the 15th and

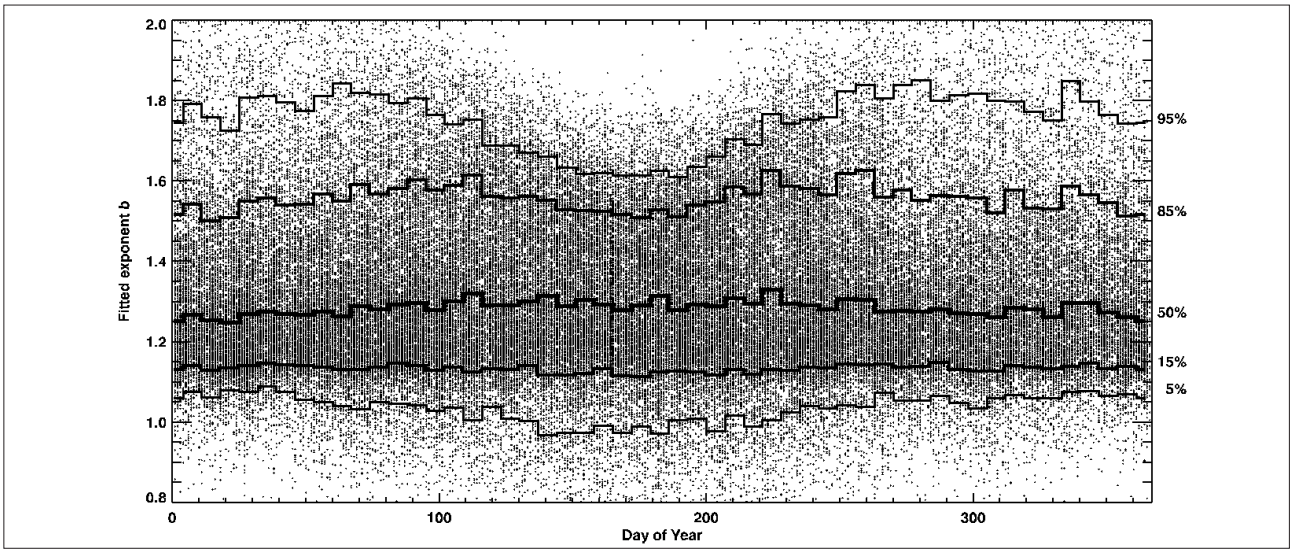

Figure 3: Fitted exponent b values by day of year for 'clear-sky' days, with weekly percentiles.

50th percentiles, as calculated weekly throughout the year (Figure 3).

Using the fixed function with b = 1.15 fitted to the full dataset, criteria of

$$I_{1.15} > 850 \text{ W m}^{-2} \quad (2)$$

$$X^2 < 0.01\, I_{1.15}{}^2 \quad (3)$$

retain about 30% of the data (121 520 site-days) as similar to clear skies. This is a considerably higher proportion than the typical 5-10% of days that are cloud-free even in locations with a high prevalence of such conditions. Further restriction is available at any stage of the subsequent analysis, but doing so for some sites with frequent scattered cloud reduces coverage markedly, especially in winter months when shorter days and lower sun angles cause more variability in $I_{1.15}$ values. Because of the wider acceptance criteria, only the higher values of $I_{1.15}$ correspond to genuinely clear days in the following plots. Note that $I_{1.15}$ is the fitted model irradiance for overhead sun, in which sense it is independent of latitude. Lower average values of $I_{1.15}$ could occur for a site with greater aerosol optical depth, especially of absorbing aerosol.

The overall time series of fitted $I_{1.15}$ since 1996 is shown in Figure 4, together with five percentiles (5,15,50,85,95) for each year. The distribution is stable until perhaps 2008, but then increases to 2012, and the change is actually monotonic from 2005. Such changes may be possible for a single site or even a region, but they are surprising for the country as a whole. Much has been written about 'Global Dimming and Brightening', whereby global (meaning hemispheric, rather than world-wide) irradiance decreased from the 1960s to around 1990 (Stanhill and Cohen 2001), then levelled off or increased after that (Wild et al., 2005). The pattern also appears in New Zealand data (Liley 2009), but mostly as an effect of diminished cloud rather than increasing clear-sky irradiance. The latter is very improbable for New Zealand as it would require reduction in absorbing aerosol by an amount much greater than the observed total aerosol burden over New Zealand prior to the increase (Liley and Forgan 2009).

To reliably quantify any such change, it is necessary to check instrument calibrations. Instruments in the NIWA

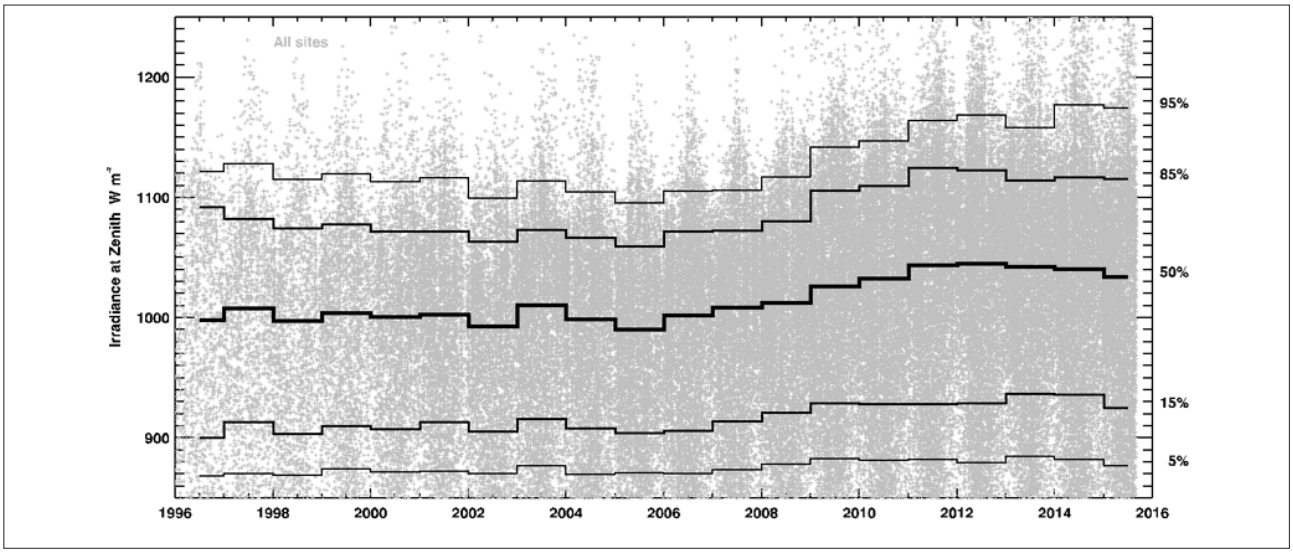

Figure 4: Fitted $I_{1.15}$ (model irradiance for overhead sun) for the 30% clearest days at all sites, since 1996, with annual percentiles.

network are deployed for up to two years, then returned for recalibration with another sensor installed. From the spreadsheet record of pyranometer calibrations and deployments, it is possible to trace which sensor was in use at any time, as illustrated in Figure 5 for Wallaceville EWS.

Figure 5 does suggest a step change of around 60 W m^{-2} in irradiance at zenith, or 5.5% in measured irradiance, occurred with the change from PSP 17857 to PSP 13996 in early 2008. Another more improbable change, with zenith values to 1250 W m^{-2}, occurred with PSP 21249 in 2014, but the #13996 values are reasonably consistent with those from #13994, #35090, and #13995 to the end of 2013.

To explore the relationship further, other reference data are needed, as available at the Lauder EWS site.

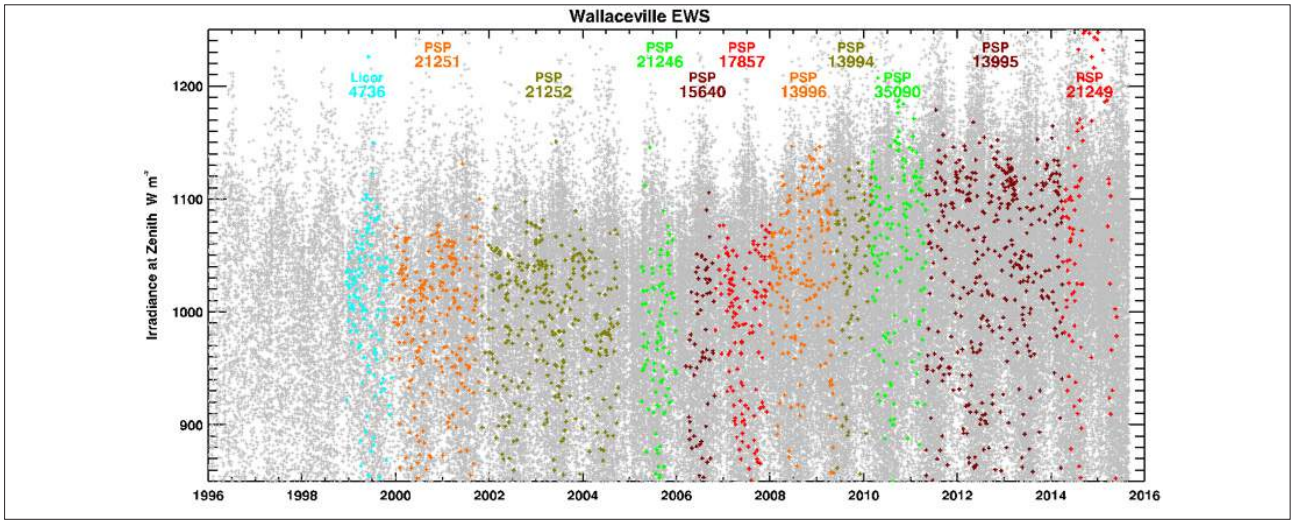

Figure 5: Fitted $I_{1.15}$ for Wallaceville EWS (CliFlo #17029, 41.135° S, 175.05° E, 56 masl), for the 30% clearest days, compared with the pattern for at all sites since 1996. Data are coloured by which sensor was in use.

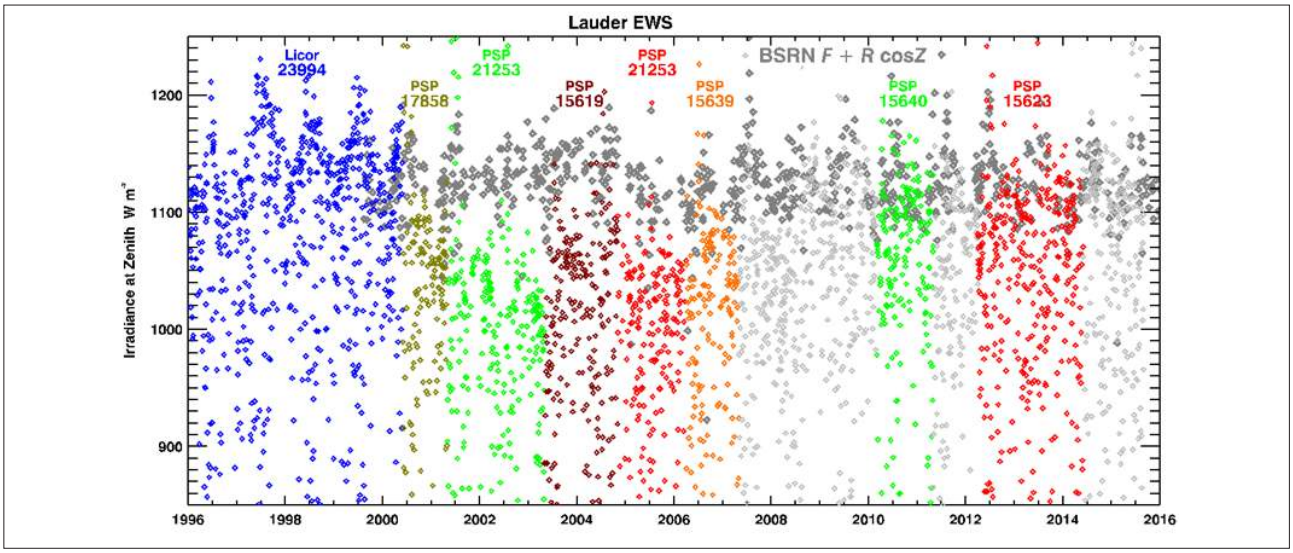

Figure 6: Fitted $I_{1.15}$ for Lauder EWS (CliFlo #5535, as in Figure 1), for the 30% clearest days, coloured by the which sensor was in use where known (i.e., excluding light grey data). The darker grey values are $I_{1.15}$ fits to hourly-aggregated values of F + R cos*Z* from BSRN data for the 12% clearest days.

There, the BSRN instrumentation includes separate measurements of global (G), diffuse (F), and direct (R) radiation at 1 Hz, reported as 1-minute observations with statistics. In accordance with BSRN practice, the primary measurement of global irradiance is not G but the sum F + R cos*Z*, which is more stable against measurement artefacts.

With 1-minute time resolution, fitting of the clear-sky model (1) is more precise, as is the fit with b = 1.15, allowing more stringent criteria for clear-sky days. Restricting from equation (3) to

$$X^2 < 0.001\ I_{1.15}{}^2 \qquad (4)$$

retains only 12% of the clearest days. Fitting the 1-minute data gives slightly higher values of $I_{1.15}$, so for comparison with the CliFlo data the BSRN were aggregated into hourly data for re-fitting, with results as shown in Figure 6.

As noted earlier, it is only the higher values of $I_{1.15}$ from the Lauder EWS data that should match the BSRN values, but it is clear from Figure 6 that the changing peak intensities in the former dataset are at odds with the latter.

Both Figure 5 and Figure 6 suggest that peak values are consistently higher or lower within the period of deployment of particular sensors, calling into doubt the calibration factors use to scale sensor signals. From the periods where the Lauder sensor is identified in the spreadsheet of calibrations, we can divide out the applied calibration factor, and replace it with the average value for that sensor. The result is shown in Figure 7.

This 'recalibration' removes much of the trend in the Lauder EWS data (with identifiable sensors), and agreement with the BSRN data is somewhat improved. On the 461 days in common from the best 12% of BSRN and 30% of EWS days, the difference between fitted irradiance at zenith has a mean of 57 W m^{-2} and s.d. of 51 W m^{-2} in the unadjusted data. Adjustment as above reduces both figures to 53 and 49 respectively. Such improvement is minor but useful, and it may be improved with higher time resolution to give better clear-sky fits.

The possible implication that the data might be more consistent without regular sensor calibration is

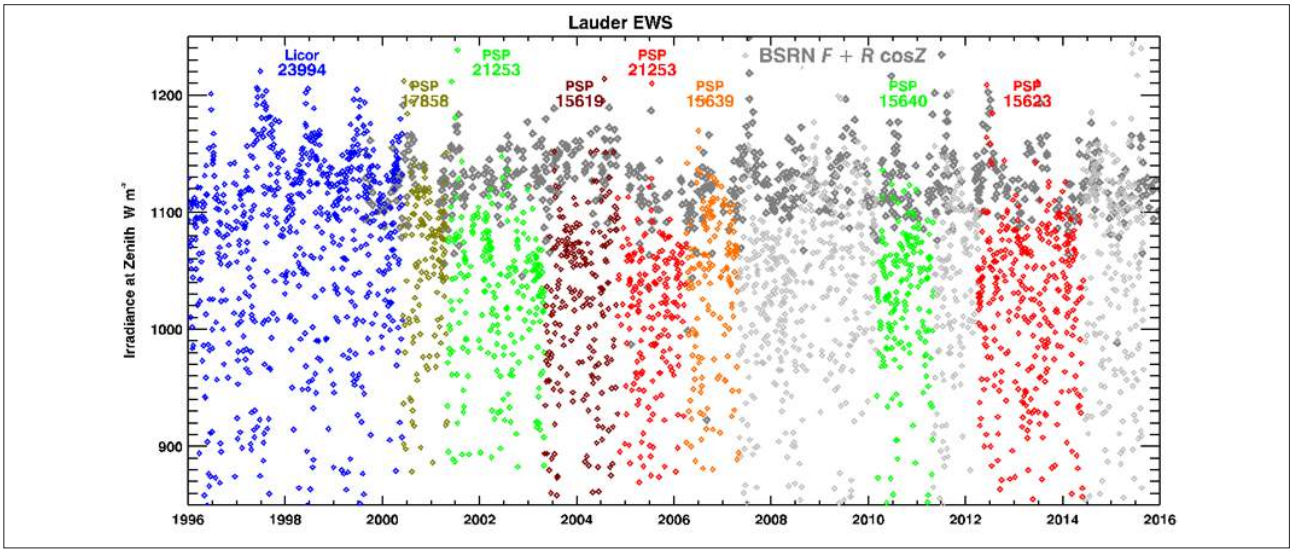

Figure 7: As Figure 6, but with fitted $I_{1.15}$ for Lauder EWS rescaled to the average calibration factor for that sensor.

disconcerting,and warrants further exploration. Figure 8 shows the calibration factors for all NIWA PSP sensors. The response of most instruments shows a gradual decline over time, as expected, with random variation that is within the 3.5% (2σ) uncertainty. That uncertainty is illustrated for two instruments (#15639 and #21250) that showed marked decline in response, necessitating their removal from use. Those instruments illustrate why regular calibration checks are necessary.

What should perhaps be reviewed is how the calibration factors are applied, but that presents some difficulty. At first deployment, only one factor is available; usually the manufacturer's calibration. After the first recalibration, there is a new figure, but any difference within the uncertainty of calibration might be random, or it might

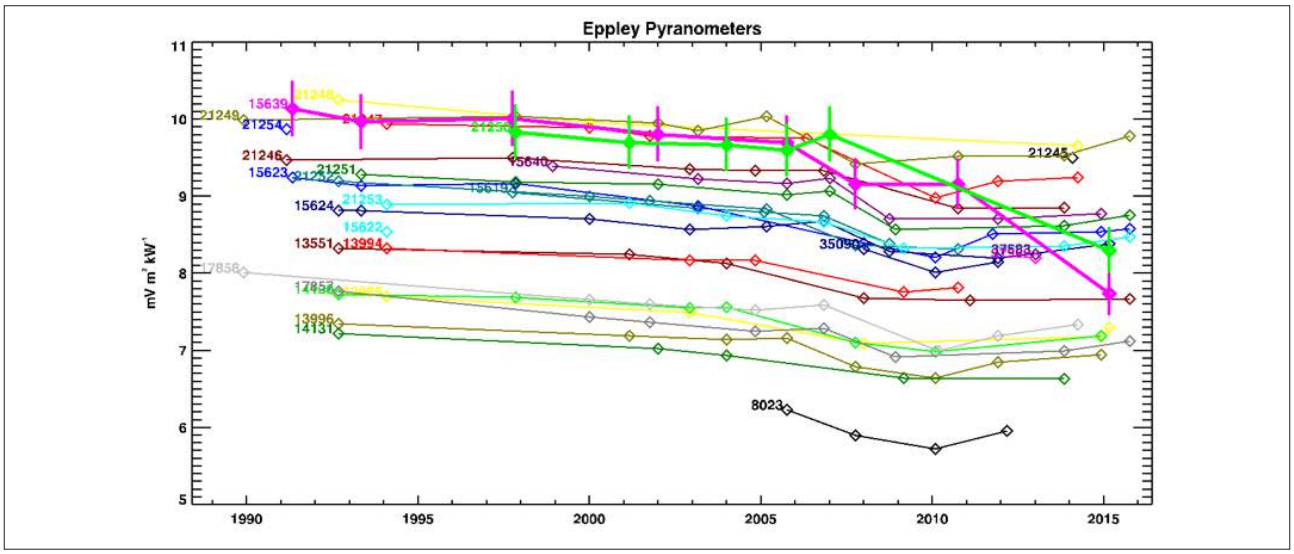

Figure 8: Calibration factors for Eppley PSPs in the NIWA calibration spreadsheet, with 3.5% (2σ) uncertainties shown for instruments #15639 and #21250, which were not redeployed because of degradation.

have some component of secular change. At present, just the new value is used to process subsequent data. Repeating this process over time for an unchanging instrument, the variance of calibrations adds to the variance of field measurements.

From statistical control theory, a better approach might be to change the applied calibration factor only when it moves outside the confidence limits of calibration, but then gradual drift would result in step changes.

There are other alternatives, such as treating the mean of all calibrations as the correct factor, or fitting a linear trend for each instrument as would be suggested by Figure 8, and revising past values. Both of these might require regular revision of past data with new calibrations, greatly confusing any analyses and quickly rendering them out of date. Another approach would be to just store voltages, and serve data along with calibration factors for users to apply. This would be awkward and confusing for many users, and it only transfers the problem of maintaining consistency with past values.

Confronted with the same issues, the satellite data community and others maintain different versions of derived data, based on retrospective recalibration or other revisions of data processing. In the context of CLIDB irradiance data, which are just scaled from sensor signals without any offset, the revision necessary for past data would be as simple as applying a factor to all measurements over a series of intervals.

Subsequent to the analysis herein, a reviewer of this paper provided a 2009 report from MetService to NIWA that appears to explain the anomalous change between 2008 and 2012. From around 1990, one of the then internationally-recommended practices implemented by NZ Meteorological Service for calibrating their Working Standards yielded factors that led to field measurements being 3-5% low; a difference of 30-50 W m^{-2} at irradiance of 1000 W m^{-2} as in Figure 4. A change in the internationally-recommended practices was implemented by MetService in 2008, thereafter progressively affecting the calibration of all network sensors, and therefore the network data collected from 2009 to 2012.

This change had a larger effect than most of the intrinsic variability of recalibration, and it affected all sensors in a similar way, introducing bias rather than just additional variance. Nonetheless, it provides a further argument for the need to support possible revision of historical irradiance data, whether for an overall correction or for applying a smoothed description of instrumental response.

What is needed is a new CLIDB metadata record type giving instrument type and serial number, deployment dates, and calibration factors as applied to the stored data. The same record type, with version, could be used for any suggested revision.

The analysis here was for Eppley PSPs, as the instruments deployed at Lauder for the period of BSRN data. Other sites may provide a similar opportunity for comparison: Paraparaumu with (corrected) data from MetService Working Standards; Kaitaia, Paraparaumu, and Invercargill with direct and diffuse data; and other sites where different agencies, especially NIWA and MetService, have sensors near to each other. They might support a comparison of Licor measurements, but the larger uncertainty in Licor data will probably reduce the statistical significance of any differences.

4. Conclusions

Fitting pyranometer data with a simple function of solar zenith angle can be used to find clear-sky days. For New Zealand's generally clean (low aerosol) atmosphere, fixing the dependence on solar zenith angles still provides a good fit, and also gives a reasonably consistent measure

of pyranometer response that can be related to calibration factors.

Applying this process across all NIWA pyranometer data suggests that some of the measured variation is spurious, probably resulting from uncertainty in the calibration procedure.

Of possible improvements to procedures to give more accurate data, the simplest will be to derive a set of suggested adjustments to be applied retrospectively. For any strategy, the one critical component is maintaining complete and accurate records of both calibrations and deployments.

Acknowledgements

Many thanks to Andrew Harper and Kyle Saywell for the vital information on calibrations and deployments, and also to Greg Bodeker for past UV Atlas work that made the pyranometer data easily accessible. I am grateful also to the reviewers for helpful comments, and to MetService for the 2009 report explaining the overall change in measured irradiances after 2008.

References

Bodeker, G. E., and R. L. McKenzie, 1996: An algorithm for inferring surface UV irradiance including cloud effects. J. Appl. Meteorol., 35, 1860-1877.

Bodeker, G. E., J. Burrowes, R. Scott-Weekly, S. E. Nichol, and R. L. McKenzie, 2002: A UV Atlas for New Zealand. UV Radiation and its Effects Workshop, RSNZ.

Bodeker, G. E., H. Shiona, R. Scott-Weekly, K. Oltmanns, P. King, H. Chisholm, and R. L. McKenzie, 2006: UV Atlas version 2: What you get for your money. UV Radiation and its Effects: an update, Dunedin, NZ, 8-9 of 102.

Forgan, B., 2009: Basic measurements of radiation at station Lauder (2006-01). M. Bureau of Meteorology Research Centre, Ed., PANGAEA.

Liley, J. B., 2009: New Zealand dimming and brightening. J. Geophys. Res., 114, D00D10.

Liley, J. B., and B. W. Forgan, 2009: Aerosol optical depth over Lauder, New Zealand. Geophys. Res. Lett., 36, L07811.

Ohmura, A., and Coauthors, 1998: Baseline Surface Radiation Network (BSRN/WCRP): New precision radiometry for climate research. Bull. Am. Meteorol. Soc., 79, 2115-2136.

Stanhill, G., and S. Cohen, 2001: Global dimming: a review of the evidence for a widespread and significant reduction in global radiation with discussion of its probable causes and possible agricultural consequences. Agric. Forest Met., 107, 255-278.

Tait, A., and B. Liley, 2009: Interpolation of daily solar radiation for New Zealand using a satellite data-derived cloud cover surface. Weather and Climate, 29, 70-88.

Wild, M., and Coauthors, 2005: From dimming to brightening: Decadal changes in solar radiation at Earth's surface. Science, 308, 847-850.

Condensation nuclei and aerosol optical depth measurements through the western Pacific Ocean

A. M. Bromley[1], M.J. Harvey[1], S. A. Gray[1] and J. McGregor[1]

[1] *National Institute of Water and Atmospheric Research (NIWA), Private Bag 14901, Wellington, New Zealand*

Correspondence: *Tony.Bromley@niwa.co.nz*

Key words: condensation nuclei, aerosol optical depth, western Pacific Ocean, aerosol source regions, back trajectories

Abstract

We present observations of condensation nuclei (CN) and aerosol optical depth (AOD) from a shipboard project using bulk-carrier ships sailing through the western Pacific Ocean between Nelson, New Zealand, and Osaka, Japan. The data is from eight voyages between 2006 and 2013.

CN counts for all voyages followed the same broad pattern: highly variable numbers near New Zealand, then variable and occasionally very high counts north of New Zealand through to the South Pacific Convergence Zone (SPCZ) and the Intertropical Convergence Zone (ITCZ). Through the north western Pacific Ocean there were generally very low counts until approaching Japan when high counts were measured in eastward outflow from Japan, Korea and China.

AOD measurements were made on voyages from 2007 at 20- minute intervals during daylight hours when the sun was clear of cloud. Back trajectories were calculated to identify airmass source regions. The AOD data were plotted in relation to the identified source regions to give estimates of aerosol size and turbidity. The AOD data was then compared to aerosol information obtained from the Moderate Resolution Imaging Spectroradiometer (MODIS) instrument onboard the Aqua earth-orbiting spacecraft.

Substantial temporal variability in fine spatial structure of the latitudinal occurrence of CN and AOD was noted. This often reflected the position and strength of the major convergence zones and the movement of synoptic-scale weather systems through the western Pacific Ocean. The aerosol data matches well with the source regions identified by back-trajectory plots. The variability in transport may be as important as variability in sources in determining the structure of CN across the western Pacific Ocean.

1. Introduction

From 2006 to 2013 measurements of condensation nuclei (CN) were made aboard MV Transfuture5, operated by the Toyofuji Shipping Company based in Nagoya, Japan. The ship sailed through the western Pacific Ocean on direct voyages between Nelson, New Zealand (41° 17' S; 174° 17' E) and Osaka, Japan (34° 40' N; 135° 30' E) at an average speed of 37 km h^{-1}. The voyage of 10,000km is completed in just under 12 days on a great circle transect

Submitted: 19 July 2018
Accepted: 28 November 2018

that runs approximately north-south across the South Pacific Convergence Zone (SPCZ) and Intertropical Convergence Zone (ITCZ). The individual voyage tracks are spatially identical, generally varying no more than 5km at any location. On the voyages from 2007 onwards shipborne aerosol optical depth data were also collected during daylight hours when the sun was clear of cloud.

Atmospheric aerosols are one of the largest sources of uncertainty in the current understanding of climate change (IPCC, 2013). They affect the climate by absorbing and scattering solar radiation (direct radiative effect), acting as cloud condensation nuclei (CCN) and hence affecting the radiative properties of clouds (indirect radiative effect). Chemical changes can occur on aerosol surfaces, altering the chemical and radiative properties of the atmosphere. Aerosol sources include biomass burning, volcanic eruptions, sea salt, biological and fossil fuel burning and aeolian dust. A secondary aerosol source originates with gas-to-particle conversion from the oxidation of organic and inorganic gaseous compounds (de Leeuw et al., 2014). A summary of aerosol data collected around the Pacific basin as part of numerous field experiments – GLOBE (Global Backscatter Experiment), ACE-1 (First Aerosol Characterisation Experiment), PEM A & B (Pacific Exploratory Mission) – has been published by Clarke et al., 2001, with emphasis on new particle production and evolution.

Quantifying the size distribution and chemical composition of aerosols is critical for estimating their impact on climate. The relatively short life-times of atmospheric aerosols and large spatial differences makes it difficult to relate the few surface-based observations to regional scales. Estimates of direct and indirect aerosol radiative effects are poorly constrained by observations, particularly in marine regions. Here, the clouds are susceptible to anthropogenic effects and the potential for indirect aerosol radiative forcing is largest.

Oceans constitute one of the single largest sources of atmospheric aerosols. Estimates have shown that around 30% of the total natural aerosol flux to the atmosphere is of marine origin and in the range of 1000 to 2000 Tg per year (Prospero et al., 1983; Andreae, 1995). Marine aerosols have two main components: primary aerosols produced over the sea surface by breaking bubbles and whitecaps, and the secondary non-sea-salt (nss) aerosols produced mostly by the chemical decomposition of dimethyl sulfide (DMS) and other organics produced by marine phytoplankton. Sub-micrometre aerosols form CCN in marine stratocumulus clouds (Charlson et al., 1987), influence the droplet size distribution and cloud albedo, and affect the visibility in the atmosphere over oceans (Fitzgerald, 1991). Mineral aerosols from continental and arid regions are also transported by winds to remote ocean locations and can be a source of trace minerals that support marine phytoplankton (Hoppel et al., 1990, Martino et al., 2014).

The western Pacific Ocean is a large ocean area that is influenced by all sources of aerosol production and transport: wave and bubble production, secondary aerosol production (especially in the southern western Pacific, an area of rich biological activity) and long-range atmospheric transport of aerosols from Australia, Indonesia and continental Asia. However, there are few in situ aerosol data for the region.

Here we explore the spatial distribution and transport using CN data collected during eight ship voyages between New Zealand and Japan and investigate likely aerosol source regions by long-range back trajectory calculations. In addition, AOD measurements were taken during daylight hours with clear sky conditions. We describe the measurement techniques specific to this study, followed by a discussion of the general meteorology through the western Pacific Ocean. The data from each of the transects are presented and detailed local meteorology is used to interpret various features of the CN data on each of the

eight voyages. We examine the data to determine if there is evidence of patterns suggestive of different populations of aerosols. We also discuss the large variations and interannual changes in the latitudinal distributions of CN and investigate the relationship with meteorological patterns.

2. Meteorological overview and aerosol climatology of the western Pacific

The atmospheric climatology of the Pacific Ocean and transportation of aerosols has been described by several researchers (e.g. Merrill, 1989; Prospero et al., 1989). The main meteorological features of the Pacific Ocean are shown in Figure 1. Complex tropical meteorology plays a major role in seasonal and latitudinal variations of aerosol content in the western Pacific lower troposphere. (Merrill et al, 1997). Observations have shown that the spatial variation in tropospheric aerosol over the equatorial western Pacific is related to the locations of the Intertropical Convergence Zone (ITCZ) and the South Pacific Convergence Zone (SPCZ) (Zaizen et al., 1996). The merger of moisture-laden trade winds in the tropical Pacific leads to the formation of the convergence zones (Vincent, 1994; Merrill et al., 1989). The ITCZ is the most persistent, lying between 2° - 12°N and crossing the breadth of the Pacific from Asia to Central America. It forms a strong barrier to direct inter-hemispheric transport. The ITCZ and SPCZ merge together in the western Pacific in the area 140°- 160°E, but separate further east with the SPCZ extending southeast towards Samoa and Tonga, and finally weakening and disappearing over the open South Pacific Ocean in the region of Easter Island (Figure 1). This constitutes a zone where two contrasting air masses (one originating from Southern Hemisphere ocean areas, the other prone to influence from a major continental landmass) meet and are mixed and carried high into the troposphere by strong convection. An extensive review of the behaviour and meteorology of the SPCZ has been published by Vincent (1994), who reports that its position and intensity vary seasonally but it is much more active and farther south in the summer months (December – February).

The summer southward shift of the SPCZ and an area known as the Subtropical Pacific High results in a

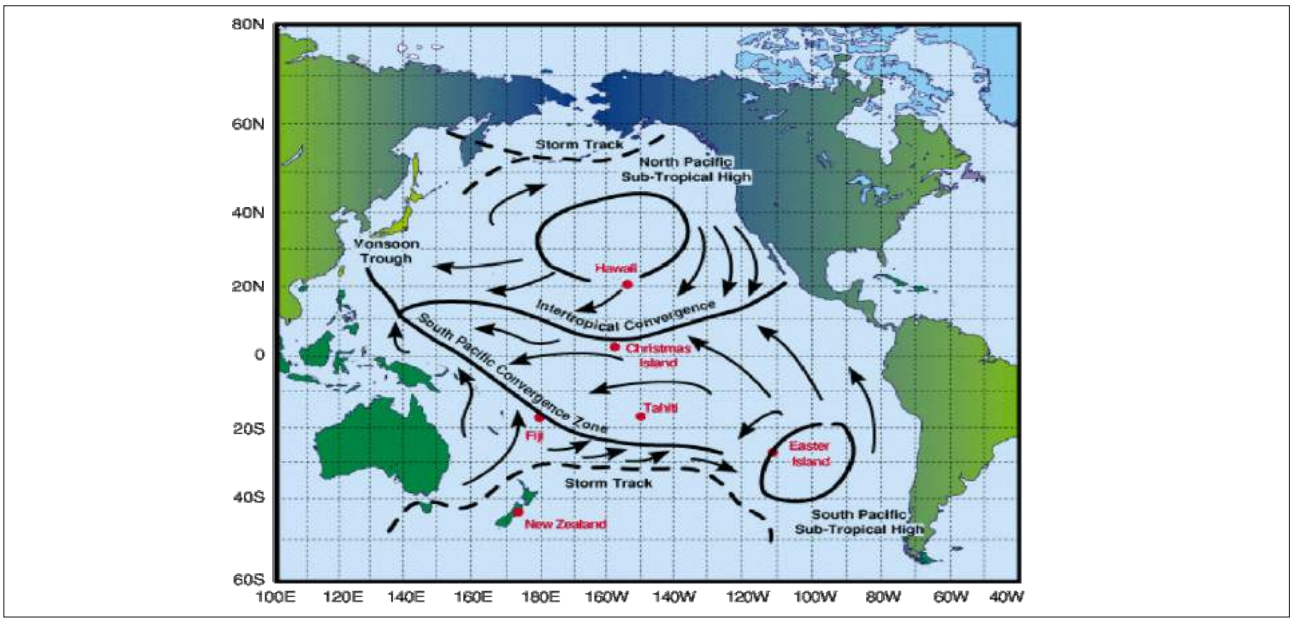

Figure 1: Main meteorological features of the Pacific Ocean (courtesy of NASA PEM-Tropics campaign).

broad region of convergence over northern Australia and eastward into the Pacific towards the Solomon Islands, producing extensive convective activity. The constant deep convection and high precipitation rates associated with the convergence zones makes accurate back-trajectory analysis difficult once the wind enters a convergence zone (Merrill, 1989). The SPCZ forms a weaker barrier to inter-hemispheric transport than the ITCZ and fluctuates seasonally in strength with major circulation changes associated with El Niño Southern Oscillation (ENSO) events. Atmospheric transport paths in the western South Pacific are less well understood than those in the North Pacific.

Southeast trade winds dominate the area north of New Zealand to 20°S and westerly winds occur on the southern side of the high-pressure belt near southern New Zealand. In winter the SPCZ migrates north and east, and south-east trade winds cover most of the southwest Pacific north of New Zealand, and westerly winds dominate between the Subtropical Pacific High and the Southern Ocean areas to the south.

North of the equator the meteorology of the lower atmosphere is dominated by two major meteorological systems in the region: the Pacific High and the Japan Jet (Merrill et al.,1997). The Japan Jet tends to be weaker and farther north in the late Northern Hemisphere summer and early autumn. During the summer/autumn period the Pacific High tends to be located more to the east and north, impeding outflow from continental Asia and enhancing the low-level flow of marine and Southern Hemisphere air into the northern mid-tropical latitudes. The northern spring period is characterised by maximum outflow from Asia, entraining emissions from the continent within a westerly flow out over the north Pacific. This flow can then swing southwards and move around the North Pacific High and bring Asian emissions into the tropical central Pacific through the northeast trade wind flows (Merrill, 1989).

In the southwest Pacific the dominant sources of aerosol mass are dust blown from the Australian continent and nss sub-micrometre aerosols produced from dimethyl sulfide (DMS) oxidation once emitted into the atmosphere following the production of precursor dimethylsulfoniopropionate by phytoplankton.

3. Shipboard sampling methodology

The Transfuture5 voyages are part of a regular trade route from the port of Nelson, New Zealand travelling directly to Osaka, Japan on a bearing of 349°T, with only a brief deviation between New Britain and Bougainville in the Solomon Islands. Each voyage was completed in 11.5 days. Although the aerosol data were collected from the commencement of the voyage, this paper discusses only the data from 30°S northwards. The data collected through the Tasman Sea off the west coast of New Zealand's North Island will be the subject of a separate paper.

NIWA's air sampling on Transfuture5 was centred on a steel shipping container attached to the top deck (deck 13). The container is located centrally, 70m from the bow and 20m aft of the crews' quarters and bridge complex. It is 100m forward of the ship's engine exhaust stack. NIWA collected the data as part of the Ships of Opportunity (SOOP) programme of the Centre for Global Environment Research of Japan's National Institute for Environmental Studies (NIES) led by Dr Y. Nojiri (Nara et al., 2011).

A TSI model 3010 condensation particle counter (CPC) sampled and counted sub-micrometre particles (>10 nm diam.) on a continuous basis. It has an upper concentration of 10,000 particles cm^3 and responds quickly to concentration changes. The CPC passes air through a heated alcohol reservoir where n-butyl alcohol condenses onto particles in the sample flow creating aerosol droplets large enough to be detected using a light-scattering technique. The sample passes into a vertical condenser tube cooled by a thermoelectric heat pump.

Here the alcohol vapour supersaturates and condenses onto virtually all particles larger than 10 nanometres in diameter, regardless of chemical composition. As droplets exit the condenser they pass through a thin ribbon of laser light. Light scattered by these droplets is collected by optics and focussed onto a photodetector which converts the light signal to an electric pulse which is recorded as a particle count.

Although the CPC is ideal for measuring very low particle concentrations, it is capable of detecting concentrations greater than 10,000 particles cm^3. The limiting factor is coincidence. The CPC counts single particles, so that each particle scatters a separate pulse of light. At high concentrations two or more particles can be in the viewing volume at the same time: the pulses they generate overlap and are counted as one particle. The frequency of this event depends on particle concentration. Within limits it is possible to determine coincidence. The coincidence correction is important at very high concentrations, but for most of the measuring range the coincidence effect is negligible. The actual particle concentration can be calculated by:

$$N_a = N_{i\,exp} (N_a QT)$$

Where N_a = actual concentration (particles cm^3)

N_i = indicated concentration (particles cm^3)

Q = 16.67 cm^3/s

T = 0.4 microsecond (the effective time each particle is in the viewing volume)

The N_a exponent can be approximated by N_i

The following table shows the calculated coincidence for a range of concentrations. Coincidence is $1-N_a / N_i$

Table 1: Calculated coincidence versus particle concentration.

Concentration (particles cm^3)	Calculated coincidence (%)
10	<0.01
100	0.07
1,000	0.67
5,000	3.5
10,000	7.4

During the voyages indicated concentrations in excess of 30,000 particles cm^3 were measured, especially just north of New Zealand. Although the actual number cannot be regarded as accurate because of high levels of coincidence, it does indicate the presence of very high particle concentration, well in excess of 10,000 particles cm^3.

The sampling intake was via a 5m ¼ inch copper tube; the inlet was located 2m above the bow end of the NIWA sampling room. The flow rate was controlled by a critical orifice with a flow rate of 1L min^{-1} and data were logged onto a computer as 30-second count accumulations. The CN concentrations were recorded as the number of particles per cm^3 of sampled air. There was no sector control used with the CPC as the intake was located 100m forward of the ship's funnel. The average speed of Transfuture5 was around 37km hr^{-1} and at this speed contamination by ship emissions was very rare and readily spotted during QC checks on the data after the voyage. In August 2006 a prolonged spell of strong south-south-east winds brought ship emissions from the engine exhaust over the CPC intake between 17.5°S and 5°S. These data have been excluded from the analysis. Occasional very short-lived periods of contamination occurred, usually of the order of one hour or less e.g. ship barbeque deck party, or lifeboat drill when combustion engines were tested. Again, these data have been excluded.

From May 2007, aerosol optical depth (AOD) data were

measured on-board Transfuture5 on all voyages as a contribution to the Maritime Aerosol Network (MAN), (Smirnov et al., 2009, 2011), a maritime extension of the Aerosol Robotic Network (AERONET). Both AERONET and MAN provide high-quality aerosol information from several hundred individual locations distributed over the Earth's surface. Additionally, satellite remote sensing has the potential to complement these networks by providing fill-in coverage between surface measurement sites and, in the case of MAN, extended temporal coverage over the oceans.

The attenuation of solar radiation through the atmosphere is described by a version of the Beer-Lambert-Bouguer law as below:

$$I = I_0 \exp(-\tau\, m)$$

Here I_0 is the incident solar irradiance at the top of the atmosphere, I the irradiance at the ground, m is the airmass factor, dimensionless path length through the atmosphere, and τ, the optical thickness of the atmosphere. At normal incidence, τ is termed optical depth. Both m and τ contain contributions from a number of absorption and scattering mechanisms, including aerosols. The aerosol contribution to optical depth, τa', termed aerosol optical depth, may be deduced from ground-based measurements of irradiance by using the above equation and correcting for the known contributions from the remaining scattering and absorbing mechanisms.

Aerosol optical depth is wavelength dependent, and for the simple case of a unimodal log-normal aerosol particle size distribution, this wavelength dependence is well described by the Angstrom relation:

$$\tau(\lambda) = \beta\, \lambda^{-\epsilon x}$$

This power law relation is specified by the two parameters, the Angstrom turbidity, β, a wavelength independent measure of optical depth, and the Angstrom exponent, α, an inverse measure of particle size. For measurements of optical depth $\tau\lambda_1$ and $\tau\lambda_2$ respectively, the Angstrom exponent is given by:

$$\alpha = -\frac{\log \frac{\tau\lambda_1}{\tau\lambda_2}}{\log \frac{\lambda_1}{\lambda_2}}$$

The Angstrom exponent is inversely related to the average size of the particles in the aerosol: the smaller the particles, the larger the exponent. Thus, Angstrom exponent is a useful quantity to assess the dominant particle size of atmospheric aerosols.

The MAN aerosol measurements of column aerosol content were obtained with a Microtops handheld sunphotometer (Porter et al, 2001); measurements were made every 20 minutes during daylight hours when the sun was clear of cloud or if the cloud cover was even and very thin cirrus. (Note that in recent times the MAN network instructions have warned to avoid any sampling through thin cirrus cloud).

4. Results and discussion

Data from eight voyages along the same transect from 2006 to 2013 are described: two each during Southern Hemisphere winter and spring, three in autumn and one in summer.

Figures 2 to 5 (a) show graphically the CPC particle concentrations (30-second count accumulations averaged over 10 minutes), absolute wind speed, ambient air temperature, relative humidity, and sea-surface temperature for each voyage by season. Temperature, humidity and wind speed were measured at deck level, 47m above sea level. The schematic above the graphed data indicates true wind direction and amounts of high,

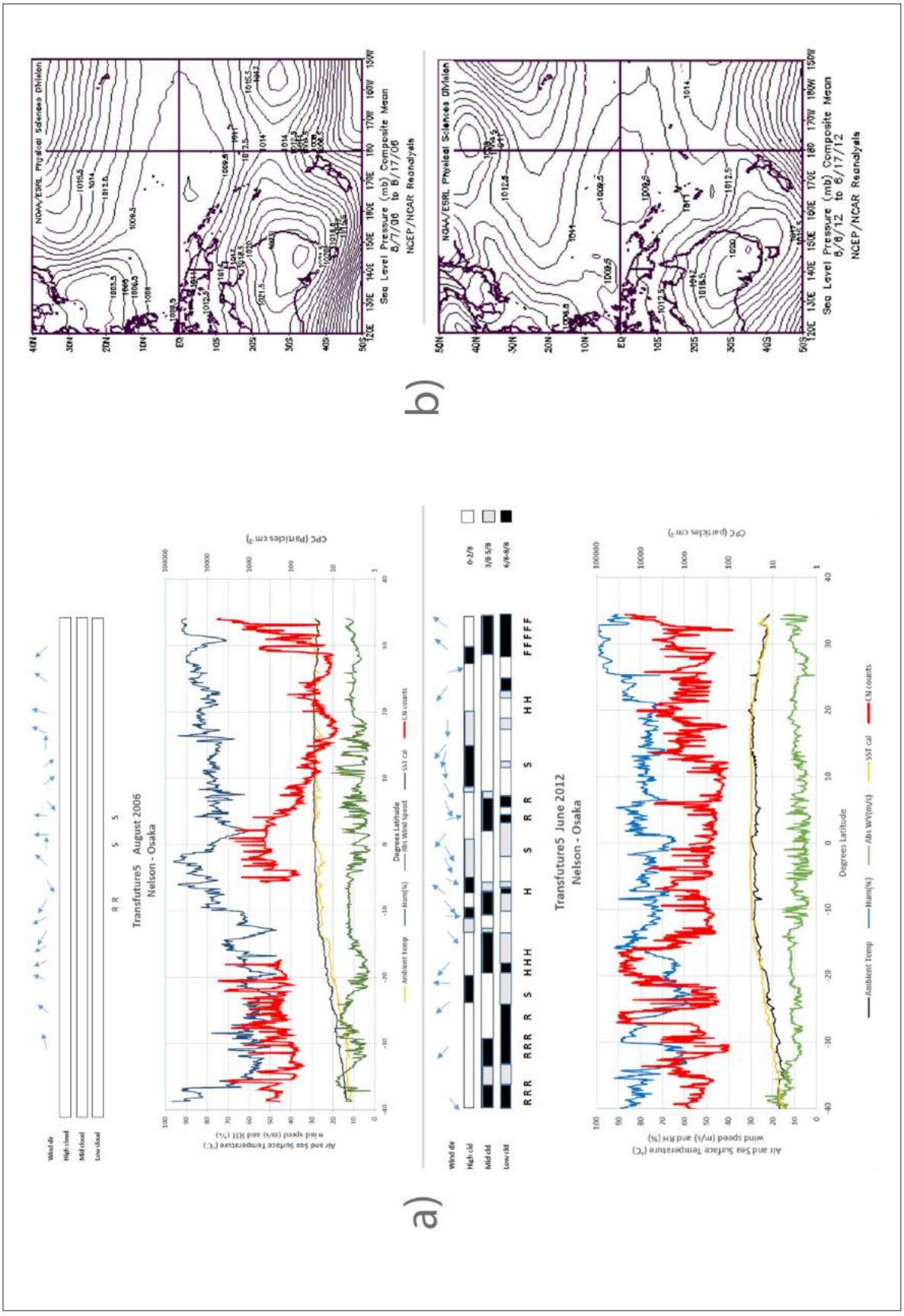

Figure 2: Winter voyages. (a) CPC particle concentrations (30-second count accumulations averaged over 10 minutes), absolute wind speed, ambient air temperature, relative humidity, and sea-surface temperature. (b) composite mean sea level (MSL) atmospheric pressure fields for each voyage by season.

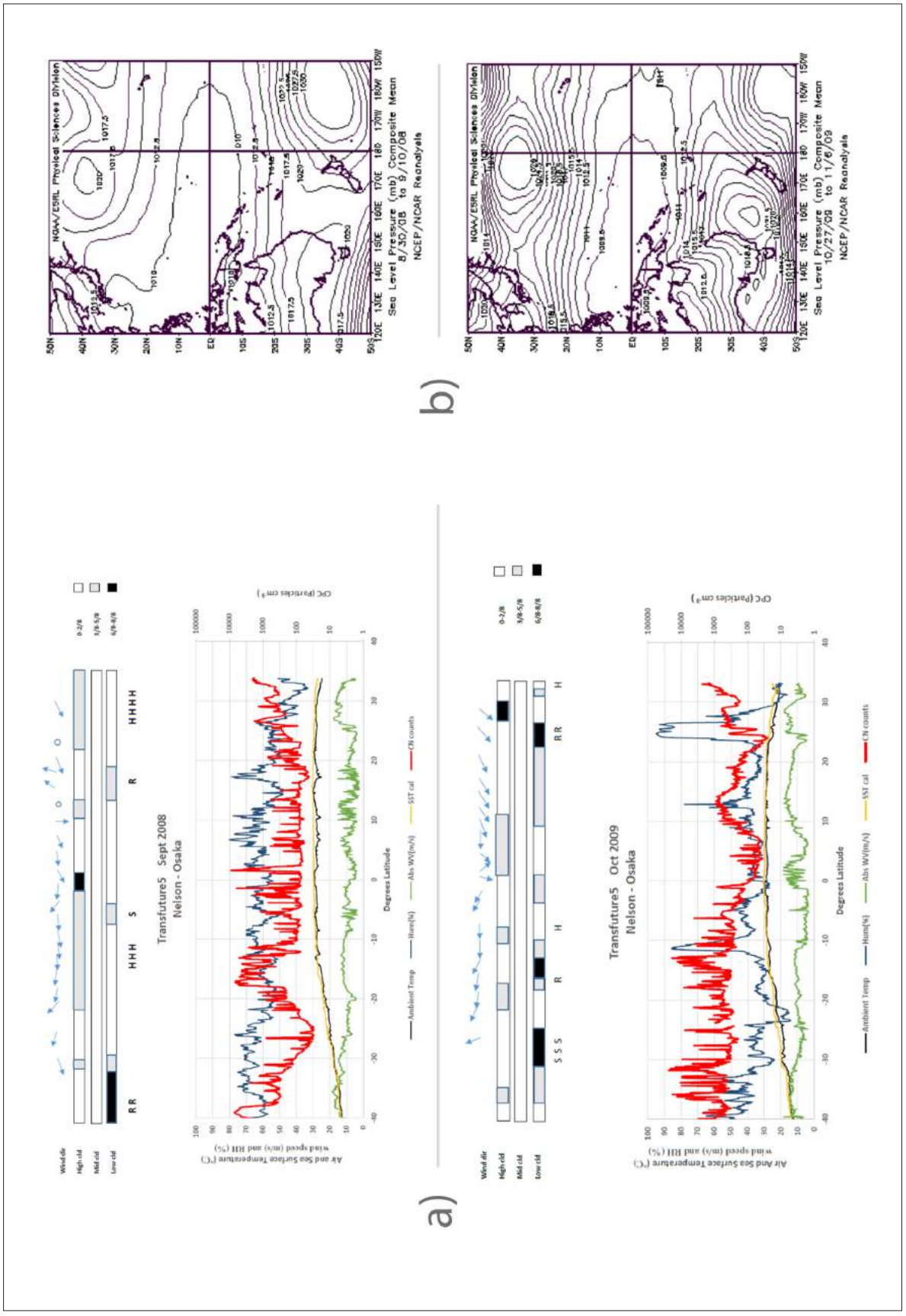

Figure 3: Spring voyages. (a) CPC particle concentrations (30-second count accumulations averaged over 10 minutes), absolute wind speed, ambient air temperature, relative humidity, and sea-surface temperature. (b) composite mean sea level (MSL) atmospheric pressure fields for each voyage by season.

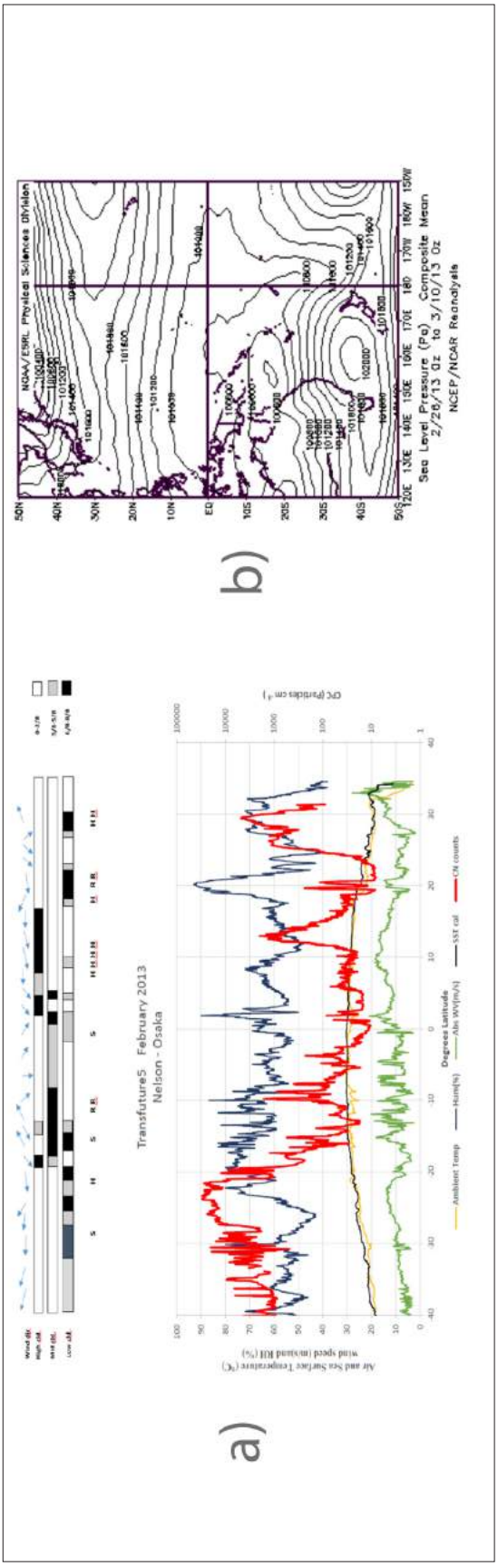

Figure 4: Summer voyages. (a) CPC particle concentrations (30-second count accumulations averaged over 10 minutes), absolute wind speed, ambient air temperature, relative humidity, and sea-surface temperature. (b) composite mean sea level (MSL) atmospheric pressure fields for each voyage by season.

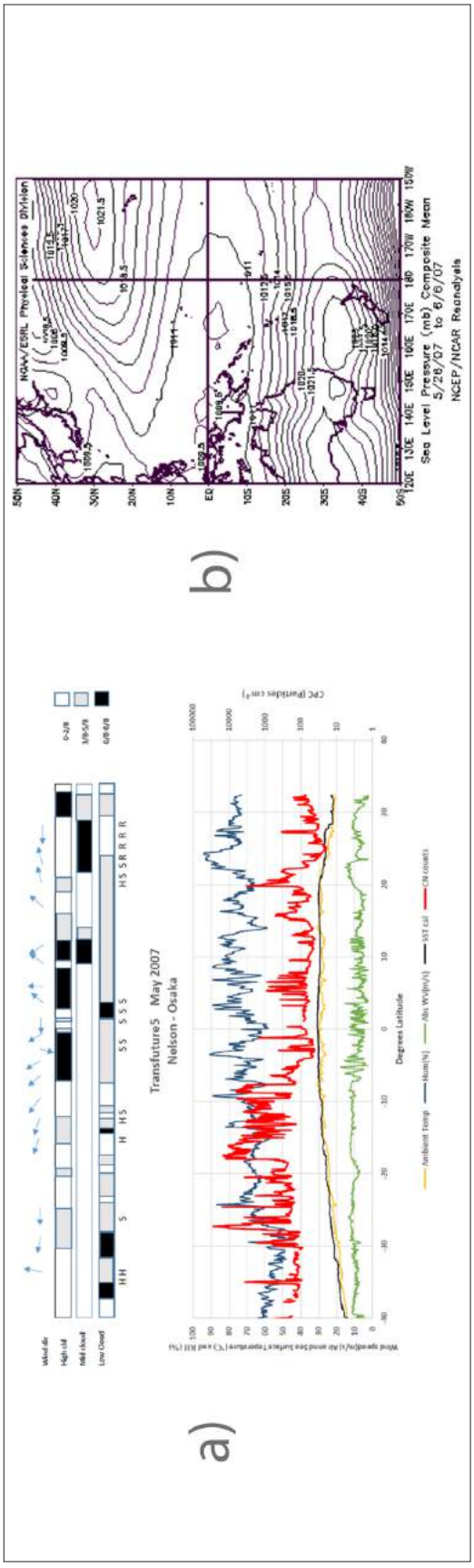

Figure 5: Autumn voyages. (a) CPC particle concentrations (30-second count accumulations averaged over 10 minutes), absolute wind speed, ambient air temperature, relative humidity, and sea-surface temperature. (b) composite mean sea level (MSL) atmospheric pressure fields for each voyage by season.

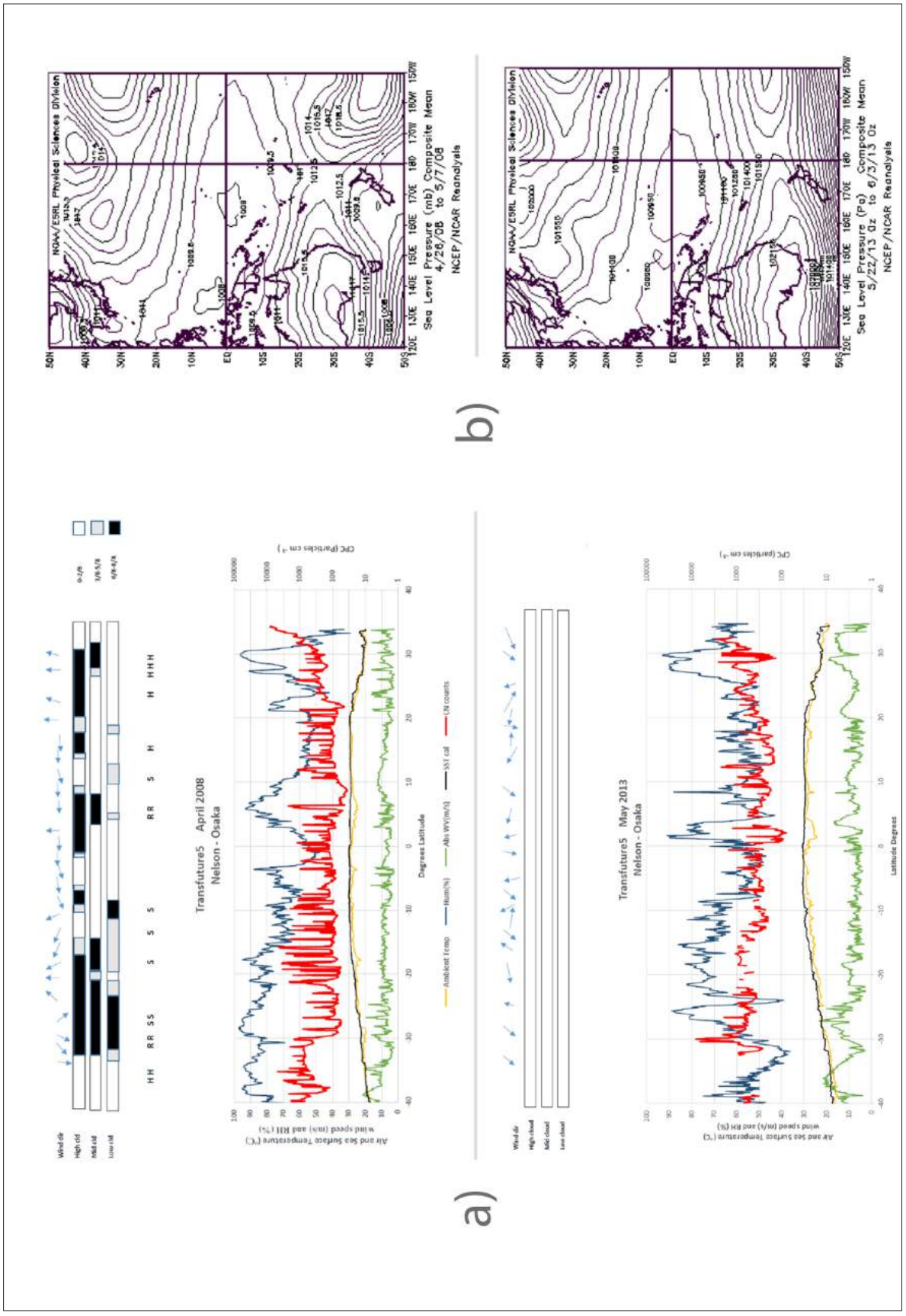

Figure 5 continued: Autumn voyages. (a) CPC particle concentrations (30-second count accumulations averaged over 10 minutes), absolute wind speed, ambient air temperature, relative humidity, and sea-surface temperature. (b) composite mean sea level (MSL) atmospheric pressure fields for each voyage by season.

middle and low cloud. Note that no cloud observations were recorded during voyages August 2006 and May 2013. The letters indicate occurrences of rain (R), showers (S), haze (H) and fog (F).

Figures 2 to 5 (b) show the composite mean sea level (MSL) atmospheric pressure fields for each voyage by season (Images provided by the NOAA/ESRL Physical Sciences Division, Boulder, Colorado from their Web site: http://www.esrl.noaa.gov/psd/) (Kainay et al., 1996). MSL patterns for each pairing of voyages are similar. Southern winter (August 2006, June 2012) has the Pacific High well to the north and east in the North Pacific, impeding outflow from Asia and bringing low-level oceanic air flow into the north-west Pacific region. Southern autumn (May 2007, April 2008) has the Pacific High in the central North Pacific, with stronger outflow from Asia into a westerly flow over the northern Pacific. Low-level oceanic flow on the southern side of the Pacific High brings easterlies into low northern hemisphere latitudes. Southern spring (September 2008, October 2009) has the sub-tropical jet stream (Japan Jet) further north and the Pacific High is still pushing a low-level oceanic flow onto eastern Asia. In all seasons, the area south of New Zealand is dominated by westerlies, while south-east trade winds cover the sub-tropical and tropical area north of New Zealand up to the region of the SPCZ.

CN counts for all voyages follow the same broad pattern: highly variable numbers in the vicinity of New Zealand, variable and occasionally high counts through the area north of New Zealand and up to the SPCZ and ITCZ. Relatively low but variable counts dominate around the convergence zones, followed by very low counts through the north-west Pacific where air has originated over low productivity / oligotrophic regions of the North Pacific Subtropical Gyre, before increasing again in the eastward outflow off Japan, Korea and China. An additional general observation was there was often an anti-correlation between CN number and high humidity excursions (April 2008, February 2013, May 2013). This phenomenon has been previously observed by McNaughton et al. (2004) in the boundary layer in Asian outflow and speculation is it could be due to the suppression of CN formation by higher surface area of coarse aerosol in high humidity, where they comment that "relative humidity approaching 100% appears to dramatically reduce the formation, growth and survival of the newly formed secondary aerosols."

The lowest counts (~10 cm^{-3}) were observed on the August 2006 and February 2013 voyages in air that had originated over the gyre region and was in or transported from the North Pacific Sub-Tropical High (Figure 1). By contrast, the June 2012 voyage was unusual in that there were consistently very high particle concentrations (>10,000 cm^{-3}) measured between 27°S and 13°S, which were thought to be due to a generally polluted airmass containing precursors and particles from industrial, and terrestrial emissions blowing off the Australian continent. Time series do also show many short duration spikes (e.g. June 2012) indicative of the occurrence of localised regions of nucleation and Aitken nuclei production. These were observed to occur downwind and in the proximity of islands with combustion and other anthropogenic activity and were often, not always absent in the northern end of the record (10° to 25°N) (e.g. see the contrast in August 2006, May 2007, October 2009). It is unlikely given the sample inlet placement but we cannot definitively exclude

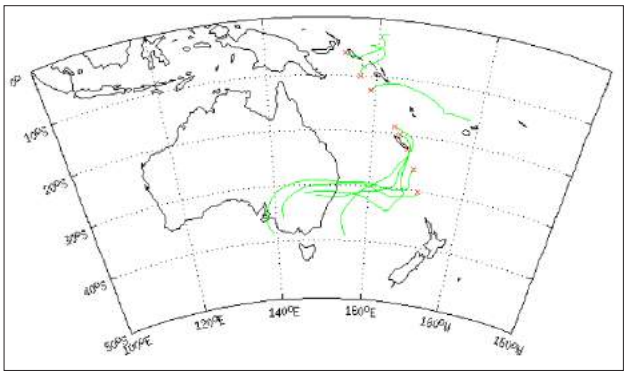

Figure 6: Back trajectory plots indicating transport of dust-laden air from SE Australia out into the western Pacific Ocean, June 2012.

local pollution of CN from the vessel as a source of some of the CN spikes. Figure 6 shows back trajectory plots indicating air measured at the ship at those latitudes had passed over southern and southeast Australia. A strong ridge of high pressure extended from Australia out over the Tasman Sea suppressing vertical mixing of the dust particles and allowing a concentrated plume to pass over the ship route north of New Zealand. Figure 13 shows AOD values associated with this air corresponding to mineral dust aerosols. Back trajectories from the May 2013 voyage (not plotted) also indicate an Australian source for the particle increase between 30.5°S and 29°S during that voyage.

4.1 Back trajectories

Air mass back-trajectories have been calculated for each voyage (HYSPLIT model via NOAA http://www.arl.noaa.gov/ready/hysplit4.html), (Draxler et al., 2003) using the Global Reanalysis 1948 – present data set as forcing meteorology to help identify the areas over which sampled air had passed. Ehhalt et al. (1999) calculated the range of residence times of tropospheric aerosols as a function of particle size (Figure 7). They point to an average CN residence time of 1-100 hours, so 4-day back trajectories were calculated.

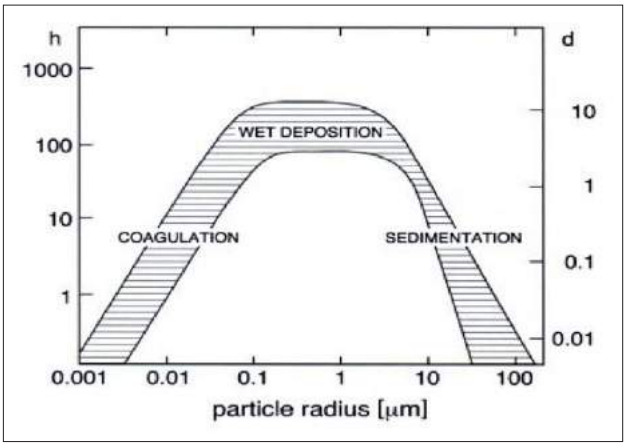

Figure 7: Range of tropospheric particle residence times (d=days, h=hours). The shaded bar shows typical range of lifetime between lower limit in the boundary-layer and upper limit at the tropopause versus size (after Ehhalt et al., 1999).

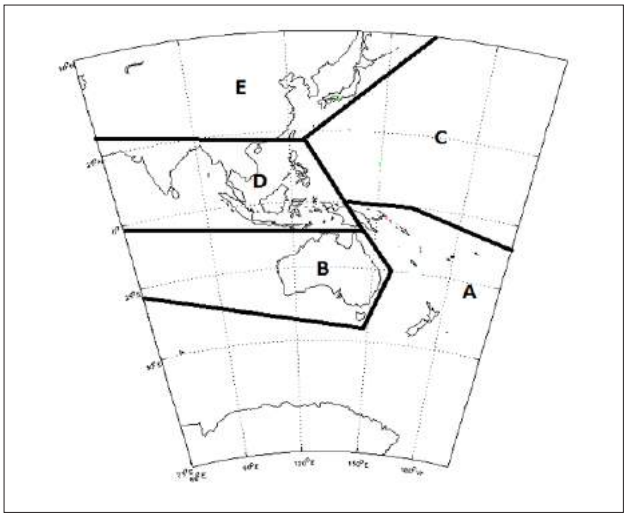

Figure 8: Airmass back trajectory region classification

We developed a system for identifying the origin of the sampled air mass: trajectory starting points were selected for times before, during and after any major change in recorded CN concentration. The trajectories were then used to classify the potential aerosol source regions. Five regions have been identified. The selected potential air mass origin classifications are shown in Figure 8.

Region A: Airflows that tend to follow the south-east trade wind regime in the South Pacific. This flow may also have spent many days over the Southern Ocean south of Australia and New Zealand before becoming entrained in the south-east trades flow.

Region B: Airflow directly from the Australian continent.

Region C: Westward airflow over the North Pacific Ocean towards south-east and continental Asia. These air masses have spent many days over open ocean but as mentioned earlier in the meteorological section, long-range transport of aerosols from Asian and North American sources can be entrained in this flow.

Region D: Outflow eastward into the North Pacific Ocean from Indonesia and Philippine Islands, with a likelihood of being influenced by industrial and domestic sources.

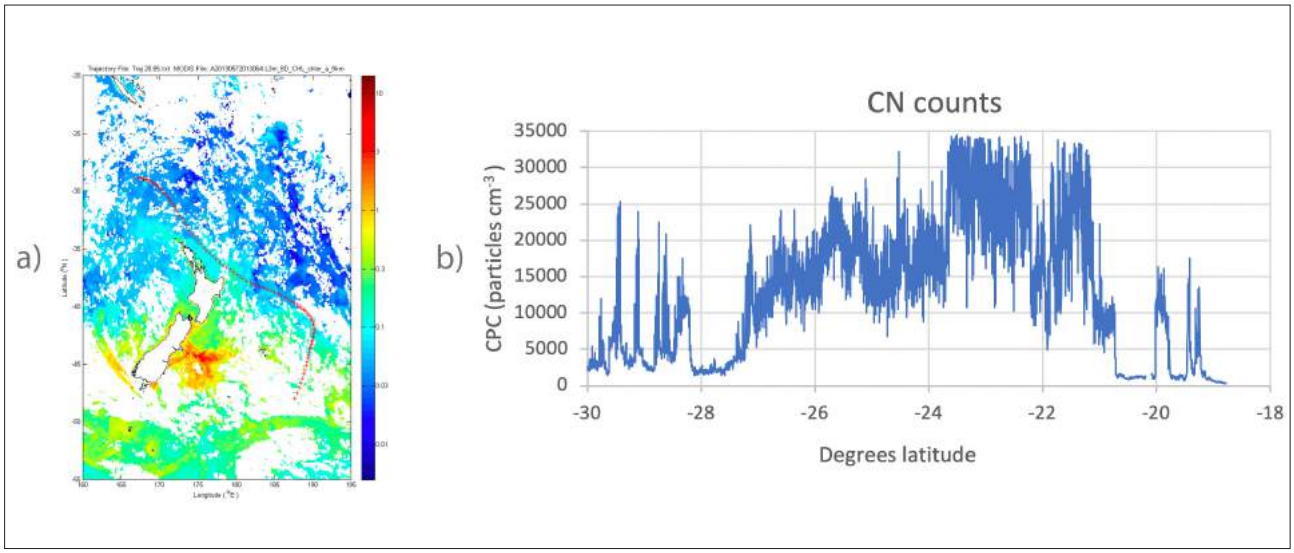

Figure 9: (a) MODIS 8-day chlorophyll-a with back trajectory plot as red dots, and (b) CN counts between 30°S and 19°S. February 2013 voyage.

Region E: Airflow associated with the eastward outflow off continental Asia, with the potential to be influenced by industrial and domestic emissions, and dust sources from the dry interior.

The airmass back trajectories at particular latitude bands are very similar for each voyage, the exception being August 2006 when surface winds north of the equator were westerlies off south-east Asia rather than the more common north-east or easterly trade winds from the central North Pacific Ocean. The air movements are consistent with the broad climatology of the Pacific described earlier and therefore representative of the region. The main airflows shown by the trajectories are similar to those found during the SEAREX programme (Merrill,1989).

Air from Region A (south-east trade winds) was encountered as far as the ITCZ, just north of the equator, and air from Region E (continental Asia) only north of 25°N. Flow from SE Asia was sampled only once, in August 2006.

4.2 Aerosol Characteristics of the source regions

Region A: This region is minimally impacted by transport of dust from continental sources. However very high particle counts in excess of 10,000 particles cm^3 have been measured just north of New Zealand on several of the voyages. These particles may well be correlated with particle formation associated with intense biogenic activity as the air passed over areas of ocean with active chlorophyll-a. VOC and DMS emissions from plankton in these areas are likely to enhance the particle concentration in the atmosphere.

In February 2013 a large spike of over 10,000 particles cm^3 in CN concentration was measured between 27°S and 21°S. MODIS satellite data showed chlorophyll-a and enhanced phytoplankton and biogeophysical chemistry activity around the New Zealand coast especially to the east of both main islands. Back trajectories showed the sampled air had travelled over an area of enhanced chlorophyll-a and it is likely the increase in CN concentration was a result of biogenic activity from this zone (Figure 9).

Another feature in most of the voyages was a CN spike in the region of 20°S. This has been attributed to particles produced by large scale open cast nickel mining in New Caledonia, and from the coal-fired power plants associated with the mining and smelting. Back trajectories indicate the sampled air had crossed the mining area before continuing out over the open ocean area. Figure 12 shows an example with trajectories indicating air passing over New Caledonia and the corresponding increase in CN between 13°S and 19°S as shown in Figure 3 September 2008 voyage data.

Some "spikiness" in the CN record occurs in the vicinity of the SPCZ and ITCZ. This is likely due to enhanced vertical motion associated with the zones, preventing extensive horizontal surface mixing of aerosols.

Region B: Australia is the major dust source in the South Pacific (Prospero et al., 1989, Martino et al., 2014). Large scale synoptic flows from Australia out into the SW Pacific are common. Much of Australia is arid, with over 4 million km^2 susceptible to severe dust storms (Loewe, 1943, Ekström et al., 2004, O'Loingsigh et al., 2017). On two voyages (June 2012 and May 2013) high concentrations of aerosols (in excess of 10,000 particles cm^3) were sampled that originated from the Australian continent. These plumes occurred in austral winter, which is the season of minimum dust activity on the Australian continent; this may imply that during the summer, when dust storm activity is more frequent, occurrences of aerosols originating from Australia may be much higher.

Region C: In general this part of the Western Pacific has low CN concentrations with prevailing winds from the easterly quarter. The air masses have had many days over open ocean and most anthropogenic sourced particles have either dropped out gravimetrically or washed out by rain. The northern spring period has maximum seasonal outflow from continental Asia, and these emissions can be entrained in this westerly flow, which can swing southwards over the eastern North Pacific and eventually move back westward into the central Pacific via the northeast trade wind flows (Merrill, 1989).

Regions D & E: These regions are densely populated areas with intensive industrial activity. Westerly flow off these regions out into the western Pacific Ocean will carry plumes of aerosols from a variety of urban and industrial sources. On the occasions the ship passed through these plumes, high CN counts were recorded. The high counts are associated with regular synoptic scale weather patterns.

4.3 Aerosol Optical Depth Measurements

Transfuture5 Microtops data are summarised in Figure 10. The Angstrom relation has been fitted to the AOD data for each sunphotometer measurement to reduce the multi-wavelength data to the two parameters, Angstrom turbidity, ß, and Angstrom component, α. For 440 to 870 nm wavelength range it gives useful discrimination of aerosol sources with values of order >2 indicating large fine mode – smoke, sulfates, 1.5 – 1.7 continental pollution, 0.4 – 0.6 maritime aerosol, and 0.0 – 0.4 mineral dust. When plotted in this two parameter ß - α space, some groupings and patterns in the data are evident, suggestive of different populations of air/aerosol being sampled. The sunphotometer data in Figure 10 is colour-coded according to source regions identified from the back trajectory calculations (Figure 8).

The most distinctive grouping is evident in the difference between air sourced from the Japan/mainland Asia region (red) affecting the western Pacific Ocean north of 20°N, and the air sourced from the two predominantly oceanic regions (blue and green). The Japan/Asia air has a combination of generally higher turbidity and higher Angstrom exponent, with the latter indicating a finer particle size. This is likely the result of dominant urban/industrial air pollution source.

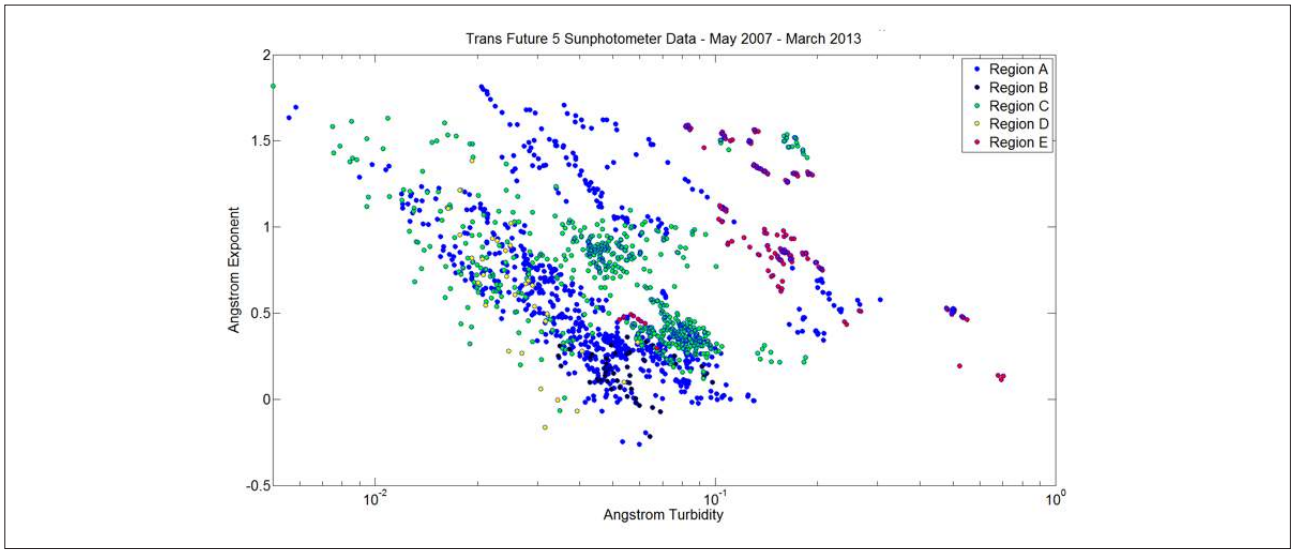

Figure 10: Combined AOD data from all voyages.

There is generally no clear distinction between sun photometer measurements of air sourced from the two oceanic regions (blue – south Western Pacific and Southern Ocean, and green – north Pacific). Both regions have similar β and α values, indicative of marine aerosol production.

In May 2007 however, there were two distinct groupings with some AOD data having abnormally high turbidity compared to the usual oceanic values (Figure 11a). Examination of the back trajectories for that voyage (Figure 11b) shows that some of the sampled air had previously passed over land regions a day or so earlier. From source region A (blue dots) some air had crossed over the Auckland area of New Zealand, the predominant urban region of that country; from source region C (green dots) air sampled near 25°N had crossed over Manila in the northern Philippines. The high turbidity AOD data is consistent with an interpretation of urban and industrial air pollution. In both cases a ridge of high pressure extending from the aerosol source region over the ship's track is likely to have suppressed the rate of particle dispersion and minimised rainout or washout, enabling a coherent plume to travel well out over the open ocean.

The September 2008 voyage AOD data shows two clearly defined groupings (Figure 12): oceanic air and air that has originated from China and Japan. Back trajectories show sampled air between New Zealand and 25°N (regions A & C) had been residing over open ocean for many days before coinciding with the ship's track (Figure 12b). The sunphotometer data show values of Angstrom turbidity and exponent that are typical of clean ocean air, in the main uncontaminated by anthropogenic sources. The data from the northwest Pacific region have a generally higher exponent value than that measured over the southern Western Pacific region (region A). North of 25°N sampled air had passed over densely populated and industrial areas of Japan and China with higher turbidity and exponent values, typical of urban/industrial pollution.

Figure 13 shows AOD data from the June 2012 voyage. A distinct grouping (circled) is associated with mineral dust particles, the sampled air having passed over south-eastern Australia as described earlier (see Figure 6).

4.4 Satellite – Transfuture5 AOD intercomparison

Satellite sensed aerosol information was obtained from

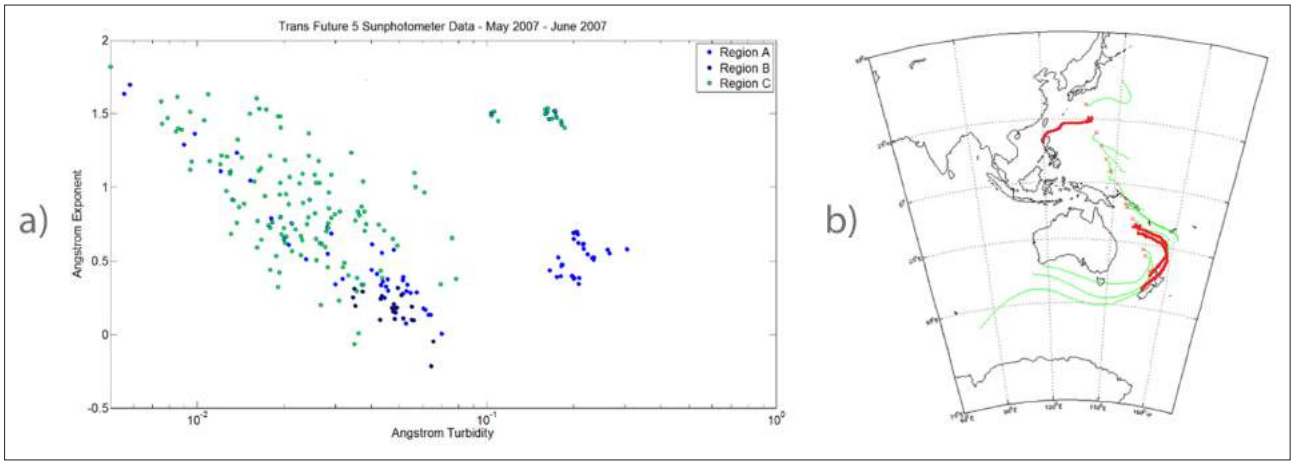

Figure 11: (a) AOD data associated with the May 2007 voyage. (b) May 2007 voyage back trajectories. Trajectories in red indicate air that has passed over large urban areas.

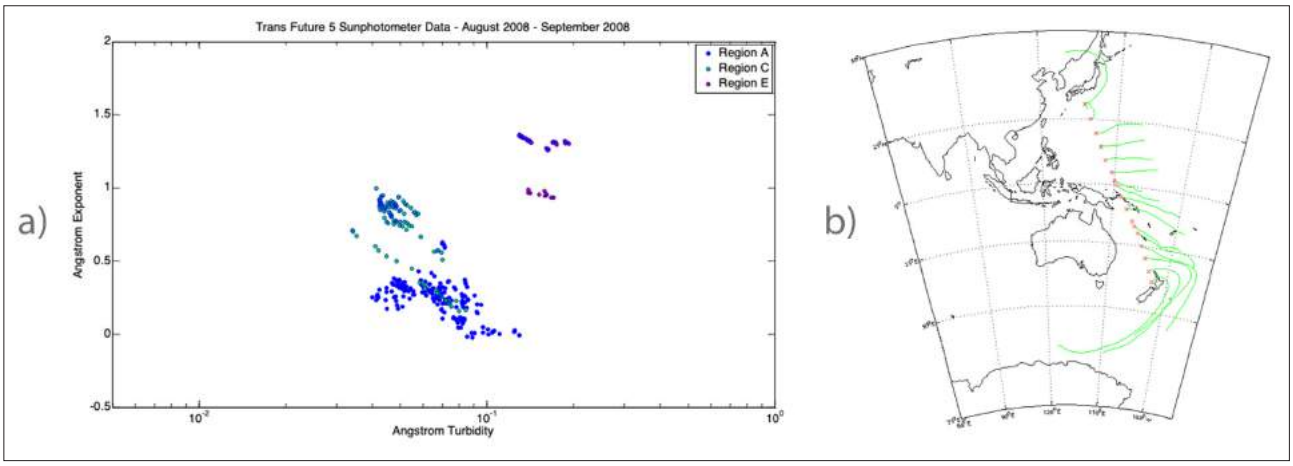

Figure 12: (a) AOD data associated with the September 2008 voyage. (b) September 2008 voyage back trajectories.

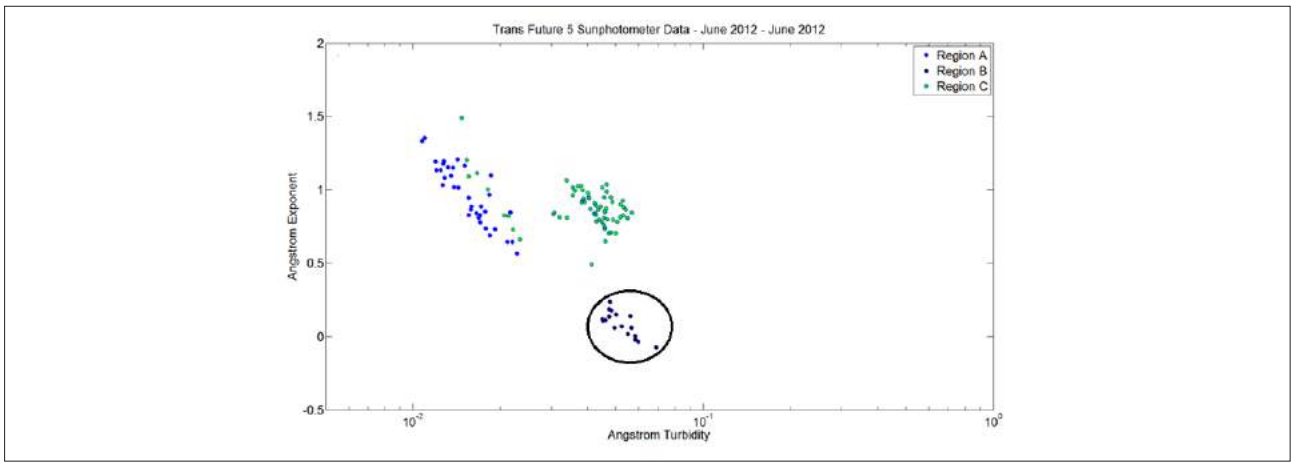

Figure 13: AOD data associated with the June 2012 voyage. The circled values indicate particles from a mineral dust source and coincide with the trajectories off Australia plotted in Fig.6.

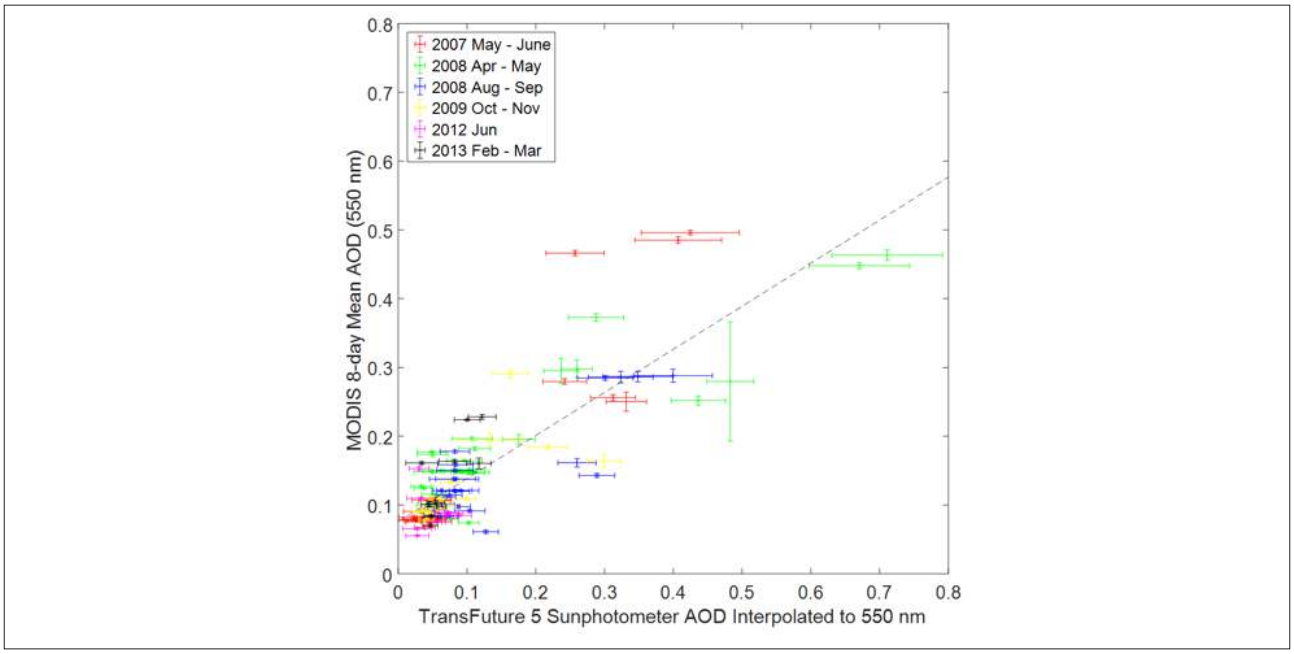

Figure 14: Transfuture5 sunphotometer data and MODIS satellite AOD data comparison.

the Moderate Resolution Imaging Spectroradiometer (MODIS) instrument flown on board the Aqua spacecraft. Aqua is in a sun-synchronous polar orbit at 705km altitude and a 98 minute period, giving global coverage. Any given point on Earth's surface will have approximately two overpasses each day.

In Figure 14, the Transfuture5 sunphotometer AOD data are compared with Aqua MODIS 8-day mean AOD. Over-ocean intercomparisons between individual MODIS images and the MAN system data are significantly constrained by the limited temporal sampling and coverage available from shipboard measurements. As the shipboard sunphotometer measurements times and locations were not chosen to coincide with Aqua overpasses, 8-day mean rather than individual MODIS AOD images were used to compensate for the lack of precise spatial and temporal co-location.

The shipboard sunphotometer measurements were grouped according to which MODIS image pixel (1°longitude x 1°latitude) they were located in; then for each pixel the sunphotometer AOD data were interpolated to the MODIS wavelength (550nm) by least squares fitting the Angstrom relation to the individual measurements. The corresponding MODIS AOD data for the group was obtained by bi-linear interpolation at the mean location of the sunphotometer group.

The resulting data shown in Figure 14 are colour coded by Transfuture5 voyage. For the MODIS data the uncertainty bars on the points are the standard deviation of the daily mean AOD, and give an indication of the variability of the AOD over the 8-day period. The uncertainty bars for the shipboard sunphotometer data are the 95% confidence limits for the Angstrom relation fit. The MODIS and shipboard sunphotometer data are in general agreement. The linear regression relation for the data is $AOD_{MODIS} = 0.63\ AOD_{TF5} + 0.076$, with a correlation coefficient of 0.85 explaining 72% of the variance.

5. Conclusions

We have presented a set of atmospheric condensation

nuclei (CN) measurements from a series of ship transects across the western Pacific Ocean from Nelson, New Zealand to Osaka, Japan between 2006 and 2013. From 2007 aerosol optical depth (AOD) measurements were made on the voyages, every 20 minutes during daylight hours when the sun was clear of cloud. Information from Hysplit back-trajectory calculations were used to identify aerosol source regions. Five distinct regions were identified: (A) the region of the south Pacific Ocean south of 10°S incorporating the south-east trade wind regime of the South Pacific and on many occasions incorporating air that may also have travelled through the Southern Ocean areas south of Australia before being entrained in the south-east trades flow; (B) the Australian continent; (C) The North Pacific Ocean; (D) south-east Asia, incorporating Indonesia and the Philippine Islands; and finally (E) continental Asia.

Substantial temporal variability in fine spatial structure of the latitudinal occurrence of CN was found. In the equatorial western Pacific Ocean this often reflected the position and strength of the SPCZ and ITCZ. However, CN counts for all voyages followed the same broad pattern: highly variable in the vicinity of New Zealand, with variable and occasionally high counts north of New Zealand as far as the SPCZ and ITCZ. Relatively low but variable counts in the areas of the convergence zones, followed by low counts through the northwest Pacific before increasing in outflow from Japan, Korea and China. These regional differences will likely influence regional differences in both direct and indirect aerosol radiative forcing.

AOD data matches well with the aerosol source regions identified by back trajectory calculations. Direct satellite – ship inter-comparisons of AOD are constrained by the difficulty in obtaining spatially and temporally co-located data. However, there is potential for the combination of satellite remote sensing, surface-based measurements from ships, and back trajectory modelling to shed light on the characteristics, distributions and probable sources of aerosols over the open ocean areas of the Earth.

We conclude that the observations of CN and AOD from the ship transects provide useful snapshots of aerosol concentrations and transport across the western Pacific Ocean. The inter-annual variability in the structure of the latitudinal changes in CN concentration suggest that long-range transport and synoptic scale weather systems are the main driver for the observed variations and that the variability in transport is at least as important as variability in sources in determining the spatial structure of CN across the western Pacific.

Acknowledgements

The authors would like to express our gratitude to the Toyofuji Shipping Company for providing passage and facilities on board Transfuture5, and her captain and crew for welcoming us on board. We also thank Y. Nojiri and Shigeru Kariya of NIES for logistical support. Mr Ross Martin of NIWA collected data on several of the voyages. Shipborne sun photometer measurements were made with the support of Alexander Smirnov though the NASA Maritime Aerosol Network.

Data

Data from the NIES Ships of Opportunity program can be accessed via: http://soop.jp

Aeronet MAN data are available through the on-line data base at: http://aeronet.gsfc.nasa.gov/new_web/maritime_aerosol_network.html

AQUA MODIS aerosol data available via: https://modis-atmos.gsfc.nasa.gov/MOD04_l2/index.html

Transfuture5 CN data available via: ftp://ftp.niwa.co.nz/tropac/MV_Transfuture5_western_pacific_CN_data/

References

Andreae, M.O., 1995. Climate effects of changing atmospheric aerosol levels. In World Survey of Climatology, 16. Future Climates of the World A. Henderson-Sellers, pp.341-392.

Boucher, O., Randall, D., Artaxo, P., Bretherton, C., Feingold, G., Forster, P., Kerminen, V.M., Kondo, Y., Liao, H., Lohmann, U. and Rasch, P., 2013. Clouds and aerosols. In Climate change 2013: the physical science basis. Contribution of Working Group I to the Fifth Assessment Report of the Intergovernmental Panel on Climate Change (pp. 571-657). Cambridge University Press.

Charlson, R.J., Lovelock, J.E., Andreae, M.O., & Warren, S.G., 1987. Oceanic phytoplankton, atmospheric sulphur, cloud albedo and climate. Nature 326 pp. 665-661.

Clarke, A.D., and Kapustin, V.N, 2002. A Pacific Aerosol Survey. Part I: A decade of data on particle production, transport, evolution, and mixing in the troposphere. Journal of Atmospheric Sciences, 59(3), pp. 363-382.

de Leeuw, G., Guieu, C., Arneth, A., Bellouin, N., Bopp, L., Boyd, P.W., Denier van der Gon, H.A.C., Desboeufs, K.V., Dulac, F., Facchini, M.C., Gantt, B., Langmann, B., Mahowald, N.M., Marañón, E., O'Dowd, C., Olgun, N., Pulido-Villena, E., Rinaldi, M., Stephanou, E.G., Wagener, T., 2014 Ocean–Atmosphere Interactions of Particles. In: P.S.Liss and M.T. Johnson (Eds). Ocean-Atmosphere Interactions of Gases and Particles. Springer Earth System Sciences: pp. 171-246. doi: 10.1007/978 3 642 25643 1_4

Draxler, R.R. and Rolph, G.D., 2003. HYSPLIT (Hybrid Single-particle Lagrangian Integrated Trajectory) Model, NOAA Air Resources Laboratory, Silver Spring, MD. Access via NOAA ARL READY Website: https://www.ready.noaa.gov/index.php

Ehhalt, D., Zellner, R., Georgii, H.W., Warneck, P., Zellner, R., Mentel, T.F. and Sausen, R., 1999. Global Aspects of Atmospheric Chemistry (Vol. 6). Springer Science & Business Media.

Ekström, M., McTainsh, G.H., Chappell, A., 2004. Australian dust storms: temporal trends and relationships with synoptic pressure distributions (1960–99). International Journal of Climatology, 24(12), pp. 1581-1599

Fitzgerald, J.W. 1991. Marine aerosols: A review. Atmospheric Environment. Part A, General Topics, Volume 25 (3), pp. 533-545.

Hoppel, W. A., Fitzgerald, J. W., Frick, G. M., and Larson, R. E., 1990. Aerosol size distribution and optical properties found in the marine boundary layer over the Atlantic Ocean, Journal of Geophysical Research: Atmospheres, 95(D4), pp.3659-3686.

Kainay,E. and Coauthors, 1996: The NCEP/NCAR Reanalysis 40-year Project. Bulletin of the American Meteorological Society, 77, pp 437-471.

Loewe, F., 1943. Dust storms in Australia. Commonwealth Meteorological Bureau Bulletin, No. 28, Melbourne.

Martino, M., Hamilton, D., Baker, A.R., Jickells, T.D., Bromley, T., Nojiri, Y., Quack, B., and Boyd, P.W., 2014. Western Pacific atmospheric nutrient deposition fluxes, their impact on surface ocean productivity. Global Biogeochemical Cycles 28 (7), pp. 712-728.

McNaughton, C.S., Clarke, A.D., Howell, S.G., Moore, K.G., Brekhovskikh, V., Weber, R.J., Orsini, D.A., Covert, D.S., Buzorius, G., Brechtel, F.J., Carmichael, G.R., Tang, Y., Eisele, F.L., Mauldin, R.L., Bandy, A.R., Thornton, D.C., Blomquist, B., 2004. Spatial distribution and size evolution of particles in Asian outflow: Significance of primary and secondary aerosols during ACE-Asia and TRACE-P. Journal of Geophysical Research: Atmospheres, 109(D19). doi:10.1029/2003JD003528

Merrill, J. T., Uematsu, M., and Bleck, R., 1989. Meteorological analysis of long range transport of

mineral aerosols over the North Pacific. Journal of Geophysical Research: Atmospheres, 94(D6), pp.8584-8598.

Merrill, J.T., Newell, R.E., and Bachmeier, A.S., 1997. A meteorological overview for the Pacific Exploratory Mission – West, Phase B. Journal of Geophysical Research: Atmospheres, 102(D23), pp.28241-28253.

Nara, H., Tanimoto, H., Nojiri, Y., Mukai, H., Machida, T., and Tohjima, Y., 2011. Onboard measurement system of atmospheric carbon monoxide in the Pacific by voluntary observing ships. Atmospheric Measurement Techniques, 4(11), pp.2495-2507.

O'Loingsigh, T., Chubb, T., Baddock, M., Kelly, T., Tapper, N.J., De Deckker, P., McTainsh, G., 2017. Sources and pathways of dust during the Australian "Millennium Drought" decade. Journal of Geophysical Research: Atmospheres, 122(2), pp.1246-1260.

Porter, J.N., Miller, M., Pietras, C., and Motell, C., 2001. Ship-based Sun Photometer Measurements Using Microtops Sun Photometers. Journal of Atmospheric and Oceanic Technology, 18(5), pp. 765-774.

Prospero, J.M., Charlson, R.J., Mohnen, V., Jaenicke, R., Delaney, A.C., Moyers, J., Zeller, W., & Rahn, K,1983. The atmospheric aerosol system – An overview. Reviews of Geophysics and Space Physics, 21(7), pp.1607-1629.

Prospero, J. M., M. Uematsu, and D. L. Savoie,, 1989. Mineral aerosol transport to the Pacific Ocean. In Chemical Oceanography, 10, pp.188– 218.

Smirnov, A., Holben, B.N., Slutsker, I., Giles, D., C.R., M., Eck, T.F., Sakerin, S.M., Macke, A., Croot, P., Zibordi, G., Quinn, P., Sciare, J., Kinne, S., Harvey, M., Smith, T., Piketh, S., Zielinski, T., Proshutinsky, A., Goes, J., Siegel, D.A., Larouche, P., Radionov, V.F., Goloub, P., Krishnamoorthy, K., Mataresse, R., J., R.E., Jourdin, F. 2009. Maritime Aerosol Network (MAN) as a component of AERONET. Journal of Geophysical Research, [Atmospheres], 114: D06204. doi: 10.1029/2008JD011257.

Smirnov, A., Holben, B.N., Giles, D.M., Slutsker, I., O'Neill, N.T., Eck, T.F., Macke, A., Croot, P., Courcoux, Y., Sakerin, S.M., Smyth, T.J., Zielinski, T., Zibordi, G., Goes, J.I., Harvey, M.J., Quinn, P.K., Nelson, N.B., Radionov, V.F., Duarte, C.M., Losno, R., Sciare, J., Voss, K.J., Kinne, S., Nalli, N.R., Joseph, E., Krishna Moorthy, K., Covert, D.S., Gulev, S.K., Milinevsky, G., Larouche, P., Belanger, S., Horne, E., Chin, M., Remer, L.A., Kahn, R.A., Reid, J.S., Schulz, M., Heald, C.L., Zhang, J., Lapina, K., Kleidman, R.G., Griesfeller, J., Gaitley, B.J., Tan, Q., Diehl, T.L. 2011. Maritime aerosol network as a component of AERONET – first results and comparison with global aerosol models and satellite retrievals. Atmos. Meas. Tech., 4(3): pp. 583-597. doi: 10.5194/amt-4-583-2011.

Vincent, D.G., 1994. The South Pacific Convergence Zone (SPCZ): A Review. Monthly Weather Review, 122, pp.1949-1970.

Zaizen, Y, Ikegami, M., Tsutsumi, Y., Makino, Y., Okada, K., Jensen, J., and Gras, J.L., 1996. Number concentration and size distribution of aerosol particles in the middle troposphere over the Western Pacific Ocean. Atmospheric Environment, 30(10-11), pp.1755-1762.

Honour Roll for the Meteorological Society of New Zealand

K. Richards

The highest level of recognition awarded by the Meteorological Society of New Zealand is Honorary Membership. This recognises outstanding contributions made by individual members to meteorology or climatology. Recognition is given to outstanding researchers, leaders in forecasting or applied climatology, and exceptional communicators, who foster Governmental and public understanding of issues in weather and climate.

The Meteorological Society has awarded ten Honorary Memberships since its inauguration in 1979. Seven recipients are profiled in the previous volume of Weather and Climate (Volume 37, 2017): the late Dr J. Thomas (Tom) Steiner (awarded Honorary Membership in 1996), the late Dr John S. Hickman, QSO (1998), Alex A. Neale (1998), the late Dr John F. Gabites (1999), Erick Brenstrum (2002), Cliff G. Revell (2002) and Dr Neil D. Gordon (2012). At the Society's Annual General Meeting in Dunedin, New Zealand in 2017, three more members joined this select group.

Robert (Bob) McDavitt, MNZM

Bob McDavitt began work as a meteorologist in 1975, forecasting for marine, aviation and the general media around New Zealand and in Fiji. In 1992, he became known as the Weather Ambassador of the Meteorological Service of New Zealand (MetService). He appeared frequently in print, radio and televised interviews to explain to the public the pattern and chaos that is weather. He has served diligently on the committee of the Meteorological Society since 1990, including in the roles of President (1998-2000) and newsletter editor (2000–). Bob retired from the MetService in 2012, but continues to post a weekly South Pacific Weather Blog for mariners. Bob was awarded the Member of New Zealand Order of Merit (MNZM) in 2013 for his outstanding service to the Crown and people of New Zealand.

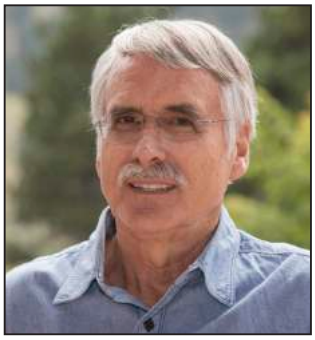

Dr. Kevin E. Trenberth

Kevin Trenberth grew up in New Zealand and started out in the New Zealand Meteorological Service. He completed a Sc.D. in Atmospheric Science-Meteorology at the Massachusetts Institute of Technology in 1972, taught at the University of Illinois, and then moved to the National Center for Atmospheric Research in 1984. He is an internationally acclaimed expert in global warming, El Niño Southern Oscillation and climate variability. He has been involved in the Intergovernmental Panel on Climate Change for many years, serving as a convening lead author and lead author for the IPCC reports and sharing in the 2007 Nobel Peace Prize. He is a fellow of the American Meteorological Society, the American Association for Advancement of Science and the American Geophysical Union, and an honorary fellow of the Royal Society of New Zealand. In 2017, the American Geophysical Union awarded him a Roger Revelle Medal for his outstanding contributions to climate and climate change research, leadership and science communication.

Brian Giles

Brian Giles spent the International Geophysical Year (1957-58) on the Argentine Islands, off the west coast of the Antarctic Peninsula, running a radiosonde unit. He then taught climatology and meteorology at the University of Birmingham, UK, until he retired in 1998. He became editor of the International Journal of Climatology in 1991. At that time, it consisted of four issues per year. By 1996, it had grown to 11 issues per year. Brian shared the editorial load with Glenn McGregor until 1999, when he moved to New Zealand. Joining the Meteorological Society of New Zealand, he served as the editor of Weather and Climate from 2003 to 2012, editing Volumes 23 to 32 (1), and continuing as publication editor until 2015 (Volume 35).